Modelling the budget of middle atmospheric water vapour isotopes

A. Zahn, P. Franz, C. Bechtel, J.-U. Grooss, T. Röckmann

Atmos. Chem. Phys., 6, 2073–2090, 2006
www.atmos-chem-phys.net/6/2073/2006/

Atmospheric Chemistry and Physics

Modelling the budget of middle atmospheric water vapour isotopes

A. Zahn[1], **P. Franz**[2,3], **C. Bechtel**[4], **J.-U. Grooß**[6], **and T. Röckmann**[2,5]

[1]Institute of Meteorology and Climate Research, Forschungszentrum Karlsruhe, Germany
[2]Max-Planck-Institute for Nuclear Physics, Heidelberg, Germany
[3]National Institute for Water and Atmospheric Research (NIWA), Wellington, New Zealand
[4]Robert Bosch GmbH, Bühl, Germany
[5]Institute for Marine and Atmospheric Research Utrecht, Utrecht University, The Netherlands
[6]Institute of Chemistry and Dynamics of the Geosphere, Forschungszentrum Jülich, Germany

Received: 11 June 2003 – Published in Atmos. Chem. Phys. Discuss.: 28 July 2003
Revised: 10 February 2006 – Accepted: 22 April 2006 – Published: 20 June 2006

Abstract. A one-dimensional chemistry model is applied to study the stable hydrogen (D) and stable oxygen isotope (^{17}O, ^{18}O) composition of water vapour in stratosphere and mesosphere. In the troposphere, this isotope composition is determined by "physical" fractionation effects, that are phase changes (e.g. during cloud formation), diffusion processes (e.g. during evaporation from the ocean), and mixing of air masses. Due to these processes water vapour entering the stratosphere first shows isotope depletions in D/H relative to ocean water, which are ∼5 times of those in ^{18}O/^{16}O, and secondly is mass-dependently fractionated (MDF), i.e. changes in the isotope ratio ^{17}O/^{16}O are ∼0.52 times of those of ^{18}O/^{16}O. In contrast, in the stratosphere and mesosphere "chemical" fractionation mechanisms, that are the production of H_2O due to the oxidation of methane, re-cycling of H_2O via the HO_x family, and isotope exchange reactions considerably enhance the isotope ratios in the water vapour imported from the troposphere. The model reasonably predicts overall enhancements of the stable isotope ratios in H_2O by up to ∼25% for D/H, ∼8.5% for ^{17}O/^{16}O, and ∼14% for ^{18}O/^{16}O in the mesosphere relative to the tropopause values. The ^{17}O/^{16}O and ^{18}O/^{16}O ratios in H_2O are shown to be a measure of the relative fractions of HO_x that receive the O atom either from the reservoirs O_2 or O_3. Throughout the middle atmosphere, MDF O_2 is the major donator of oxygen atoms incorporated in OH and HO_2 and thus in H_2O. In the stratosphere the known mass-independent fractionation (MIF) signal in O_3 is in a first step transferred to the NO_x family and only in a second step to HO_x and H_2O. In contrast to CO_2, O(^{1}D) only plays a minor role in this MIF transfer. The major uncertainty in our calculation arises from poorly quantified isotope exchange reaction rate coefficients and kinetic isotope fractionation factors.

Correspondence to: A. Zahn
(andreas.zahn@imk.fzk.de)

1 Introduction

Water vapour (H_2O) belongs to the most important trace gases in the Earth's atmosphere. It plays a key role for numerous homogeneous and heterogeneous chemical reactions (Lelieveld and Crutzen, 1990, 1994) as well as for the short-wave and long-wave radiative budget of the atmosphere (IPCC, 2001). Its extremely complex atmospheric cycle is not understood in sufficient detail, in particular since atmospheric water is present in the gaseous, liquid, and solid phase.

The interest in middle atmospheric H_2O was further intensified following observations made by Oltmans and Hofmann (1995) and after this by others (SPARC, 2000, and references therein; Rosenlof et al., 2001) who found increasing H_2O concentrations of 30–150 nmol/mol yr^{-1} in the middle atmosphere since 1954. Not only the possible causes of this trend but also the consequences for Earth's climate and the chemistry of the middle atmosphere are a matter of vital discussion (Forster and Shine, 1999, 2002; Kirk-Davidoff et al., 1999; Stenke and Grewe, 2004; Röckmann et al., 2004).

To date primarily H_2O concentration measurements, supported by atmospheric circulation models, have been used to place constraints on the hydrological cycle in the middle atmosphere (Dessler et al., 1995; Rosenlof et al., 1997; Randel et al., 2001). Independent information can be gained from the analysis of the isotopic composition of water vapour.

The isotope ratios in water vapour are usually reported as per mil deviation of the ratio "rare isotopologue" to "most abundant isotopologue" relative to the Vienna Standard Mean Ocean Water (V-SMOW) reference, e.g. $\delta^{18}O(H_2O) = (R_{^{18}O,\,sample}/R_{^{18}O,\,V-SMOW} - 1)\cdot 1000‰$, where $R_{^{18}O}$ denotes the isotopologue ratio $H_2{}^{18}O/H_2{}^{16}O$ of a sample or V-SMOW, respectively. $R_{D,\,V-SMOW}$ is $0.31152\cdot10^{-3}$ (Hagemann et al., 1970; DeWit et al., 1980; Tse et al., 1980), $R_{^{17}O,\,V-SMOW}$ is $0.3799\cdot10^{-3}$ (Li et al., 1988), and $R_{^{18}O,\,V-SMOW}$ is $2.0052\cdot10^{-3}$ (Baertschi, 1976). All δD,

Published by Copernicus GmbH on behalf of the European Geosciences Union.

$\delta^{17}O$, and $\delta^{18}O$ values in this paper are given with respect to V-SMOW.

The major source of atmospheric water vapour is the ocean having an isotope composition close to V-SMOW, i.e., $\delta^{18}O(H_2O)\approx 0‰$. Evaporation into the atmosphere leads to depletion in the rare H_2O isotopologues relative to to $H_2{}^{16}O$, due to their lower vapour pressure compared to $H_2{}^{16}O$, the vapour pressure isotope effect (v.p.i.e.). Typically, $\delta^{18}O(H_2O)$ is $-12‰$ and $\delta D(H_2O)$ is $-85‰$ just above the ocean (Rozanski et al., 1993). Cooling during upward air movement causes cloud formation and (due to the v.p.i.e.) preferential condensation and subsequent removal of the rare H_2O isotopologues by precipitation. The D/H, $^{17}O/^{16}O$, and $^{18}O/^{16}O$ isotope ratios in H_2O thus decrease with altitude and reach tropopause values in the range of $\delta D(H_2O)\approx$–(450–750)‰, $\delta^{17}O(H_2O)\approx$–(30-70)‰, and $\delta^{18}O(H_2O)\approx$–(60–130)‰, respectively (see Sect. 2). This isotopically depleted water vapour is transported to the stratospheric overworld, almost exclusively within the tropics (Holton et al., 1995; Highwood and Hoskins, 1999).

There and in contrast to the troposphere, chemical reactions considerably modify the isotope composition of the water vapour imported from the troposphere such as: (i) methane (CH_4) oxidation, the main in situ source of H_2O in the stratosphere, (ii) exchange of oxygen atoms with molecular oxygen and ozone via the HO_x and NO_x family, and (iii) oxygen isotope exchange reactions e.g. between H_2O and OH (Greenblatt and Howard, 1988; Masgrau et al., 1999). Importantly, all of these processes enrich the water vapour imported from the troposphere in the rare isotopes.

Using a one-dimensional (1-D) model we show in this paper, how these chemical reactions modify the stable isotope composition of middle atmospheric H_2O and how H_2O isotope observations may be exploited to infer constraints on these reactions and on the budget of stratospheric water. Four previous model studies on the isotopic composition of stratospheric H_2O have been made. Kaye (1990) first studied $\delta^{18}O(H_2O)$ in the middle atmosphere and suggested a significant increase in $\delta^{18}O(H_2O)$ with altitude due to ^{18}O-rich excess water from CH_4 oxidation. Ridal et al. (2001) and Ridal (2002) focused on $\delta D(H_2O)$ in the stratosphere. They found a strong vertical increase of $\delta D(H_2O)$, also due to CH_4 oxidation which is additionally modulated by the seasonally varying H_2O input from the troposphere (the "tape recorder effect"). Johnson et al. (2001a) applied a simple photochemical model with many simplifications, but inferred excellent agreement with own $\delta D(H_2O)$ and $\delta^{18}O(H_2O)$ balloon-borne observations conducted between 1989 and 1997.

The major difference of the present model study compared to earlier work is first that all three stable isotope signatures $\delta D(H_2O)$, $\delta^{17}O(H_2O)$, and $\delta^{18}O(H_2O)$ both in the stratosphere as well as in the mesosphere are combined, and second that a large number of isotope exchange reactions and all isotope fractionation coefficients measured so far are considered. Special emphasis is put on the specific pathways of D, ^{17}O, and ^{18}O from their reservoir species CH_4, H_2, O_2, and O_3 into the end product H_2O.

2 Available stable isotope data of H_2O

Due to the difficulty to measure the isotopic composition of stratospheric water with sufficient accuracy, only a limited number of H_2O isotope data have been gathered so far, which are grouped in the following according to the analytical technique employed.

(i) Most stable isotope H_2O data were collected using remote-sensing infrared spectroscopy techniques (Abbas et al., 1987; Carli and Park, 1988; Guo et al., 1989; Dinelli et al., 1991, 1997; Rinsland et al., 1984, 1991; Stowasser et al., 1999; Johnson et al., 2001; Kuang et al., 2003). They all reveal strong depletions of $\delta D(H_2O)$ with respect to V-SMOW which significantly decrease with altitude, from about $-(660 \pm 80)‰$ at the tropical tropopause (Moyer et al., 1996; Johnson et al., 2001; Kuang et al., 2003; McCarthy et al., 2004) to typically $-(450 \pm 70)‰$ at 40 km. Observations by Stowasser et al. (1999) showed extreme $\delta D(H_2O)$ depletions as low as –830‰ at 17 km inside the Arctic vortex, which was attributed to condensation and subsequent sedimentation of polar stratospheric cloud (PSC) particles.

For $\delta^{17}O(H_2O)$ and $\delta^{18}O(H_2O)$, most studies report values between 0 and –100‰ and a weak vertical increase. However, this increase is mostly not significant due to the large measurement uncertainties of 50–120‰. In contrast, early observations by Guo et al. (1989) showed increasing $\delta^{18}O(H_2O)$ values from $(80 \pm 140)‰$ at 22 km altitude to $(400 \pm 250)‰$ at 37 km. Using a balloon-borne spectrometer, Johnson et al. (2001) obtained low isotope ratios of –(300-30)‰ (average: –128‰) for $\delta^{18}O(H_2O)$, and of –(400-0)‰ (average: –84‰) for $\delta^{17}O(H_2O)$ at 12–20 km altitude.

(ii) Cryogenic in situ sampling and subsequent laboratory-based mass spectrometry (MS) analysis constitutes the potentially most accurate technique, but suffers from the very small sample amounts available and their difficult handling and MS analysis. Most observations are from the upper troposphere and lowermost stratosphere (Ehhalt, 1974; Smith, 1992; Zahn et al., 1998; Zahn, 2001) and to date there is only one set of balloon-borne stratospheric $\delta D(H_2O)$ profiles available (Pollock et al., 1980). These data likewise show a continuous increase in $\delta D(H_2O)$ with altitude, from about –450‰ at 25 km to about –360‰ at 35 km.

The single investigation on the oxygen ($\delta^{17}O$ and $\delta^{18}O$) isotope composition of stratospheric H_2O samples was conducted by Franz and Röckmann (2005) using samples obtained between New Zealand and Antarctica in August/October 2004 at altitudes of up to $\sim$5 km above the local tropopause. The data show an increase of $\delta^{18}O$ concomitant with decreasing H_2O mixing ratios above the local tropopause. This was interpreted as mixing of tropospheric and stratospheric overworld air in the high latitude

lowermost stratosphere. Notably, the data show no oxygen isotope anomaly with very small errors of $\Delta^{17}O(H_2O) < 2‰$.

(iii) In situ infrared laser spectroscopic techniques are challenging, potentially very accurate and may additionally offer high spatial resolution. First applications on board aircraft have been reported.

Using the tunable diode laser absorption spectrometer (TDLAS) ALIAS on board the high-flying NASA WB-57 aircraft, Webster and Heymsfield (2003) observed (expectedly) decreasing δD, $\delta^{17}O$, and $\delta^{18}O$ values in H_2O with increasing height up to the tropical tropopause. The high temporal resolution measurement also revealed a very high degree of variability, e.g. δD values ranging from 0 and $-900‰$ near the tropopause and clearly different values for ice and gas water, respectively. Surprisingly, the mean $\delta D{:}\delta^{18}O$ ratio for this data set is only <3 in the lower stratosphere.

In May 2004 Kerstel, Romanini, and Jost applied a cavity-ring-down technique (off-axis cavity enhanced absorption spectroscopy, OF-CEAS) on-board a DC-10 aircraft at altitudes of up to 13 km. They reported on excellent measurement uncertainties of below 10‰ for all three stable isotopologues over a certain 10 min sampling interval with particular constant H_2O mixing ratios of $\sim$200 ppmv (personal communication).

High measurement accuracies are reported by Keutsch et al. (Havard University) who measured δD and $\delta^{18}O$ in H_2O at altitudes of up to 20 km in autumn 2004 by using off-axis integrated cavity output spectroscopy (OF-ICOS) on-board the NASA WB-57. On the same flights a photofragment laser-induced fluorescence (LIF) technique were applied for measuring δD in H_2O by Hanisco et al. (Havard University) with similarly low measurement uncertainty.

3 Information provided by the H_2O isotopic composition

The isotopic composition of tropospheric water vapour is controlled by the hydrological cycle. Hence, H_2O isotope data can be used as tracers for the condensation history of probed air masses (Taylor, 1984), e.g. for studying the transport of tropospheric H_2O into the lowermost stratosphere (Zahn, 2001).

Both, $\delta D(H_2O)$ and $\delta^{18}O(H_2O)$ are primarily determined by the v.p.i.e. (see Sect. 1) and thus undergo similar variations. Indeed, in surface precipitation both isotopologues are closely related by the meteoric water line (MWL): $\delta D(H_2O) \approx m \times \delta^{18}O(H_2O) + 10‰$, with $m \approx 8$ (Craig, 1961). This relationship was found to hold reasonably well even on Mount Logan (Canada) at 5951 m altitude, with $m=7.5$ (Holdsworth et al., 1991). At cold temperatures as encountered in the tropical tropopause layer (TTL), however, kinetic isotope fractionation during formation of ice cloud particles, their lofting in convective cells and mixing of air masses with different H_2O isotope compositions are assumed to considerably reduce $\delta D(H_2O)$ depletion compared to $\delta^{18}O(H_2O)$ (Moyer et al., 1996; Keith, 2000; Johnson et al., 2001; Kuang et al., 2003; Dessler and Sherwood, 2003). In fact, using the isotope composition of water vapour entering the stratosphere of $\delta D(H_2O) = -679‰$ and $\delta^{18}O(H_2O) = -128‰$ as measured by Johnson et al. (2001), a mean slope $m=5.4$ is calculated. Due to the mass-dependent nature of isotope fractionation processes in the troposphere, $\Delta^{17}O(H_2O)$ is set to 0‰ at the tropical tropopause. Potential deviations from this assumption e.g. owing to an interplay of equilibrium and kinetic isotope fractionation factors with different three-isotope relationships (Eq. 1) were not observed yet and thus are not considered.

In this paper, we define mass-independent fraction (MIF) by using the formulation

$$\Delta^{17}O = [\ln(1+\delta^{17}O/1000) - \lambda \cdot ln(1+\delta^{18}O/1000)] \cdot 1000‰ \quad (1)$$

suggested by Miller (2002) which quantifies the deviation from mass-dependent fractionation without approximation. As three isotope exponent we adopt $\lambda=0.528$ (± 0.0015) as measured by Meijer and Li (1998) in a large number of natural waters showing $\delta^{18}O(H_2O)$ values between -50 and +10‰. This value is very close to $\lambda=0.529$ derived by Young et al. (2002) for equilibrium fractionation processes, but larger than $\lambda=0.513$ inferred for kinetic fractionation processes. It is not known to date, if kinetic fractionation during the upward transport to the tropopause results in significantly lower λ values for H_2O at the tropopause. Assuming $\delta^{18}O(H_2O) = -128‰$ at the tropical tropopause and $\lambda=0.513$ (which is also the λ value for O_2), Eq. (1) leads to only 2.05‰ lower $\delta^{17}O(H_2O)$ values. This in an exaggerated upper limit, since λ is certainly not that different for the entire condensation history. In any case, such a shift would not alter much our model results.

In conclusion, it can be presumed that tropospheric water vapour entering the stratosphere at the tropical tropopause on average exhibits a $\delta D(H_2O)/\delta^{18}O(H_2O)$ ratio of 5–6 and is mass-dependently fractionated (MDF). Possible local deviations from these two assumptions, e.g. assumed to occur in the outflow of a deep convection cells will be negligible for the H_2O isotope budget and are not considered here.

In the stratosphere chemical reactions modify this isotope signature imported from the troposphere, as will be pointed out briefly below and explained in more detail later:

(i) The first "chemical" mechanism is the in-situ source of H_2O, the oxidation of methane (and H_2). Methane is oxidized in the middle atmosphere by reactions with OH, Cl, and $O(^1D)$, and by photolysis (Lary and Toumi, 1997). Each oxidized CH_4 molecule leads to the net formation of almost two H_2O molecules (Evans et al., 1999; Zöger et al., 1999; Michelsen et al., 2000). The δD value of the produced H_2O molecule $\delta D(H_2O)$ differs from $\delta D(CH_4)$, because the CH_4 loss reactions are accompanied by unusually strong kinetic isotope fractionation. For instance, at room temperature the D isotope fractionation factor KIE^D, that is the ratio of the

rate constants $k(CH_4)/k(CH_3D)$, is $KIE^D(OH)=1.29$ for the reaction of CH_4 with OH, $KIE^D(Cl)=1.51$ for the reaction with Cl, and $KIE^D(O(^1D)=1.11$ for the reaction with with $O(^1D)$ (Saueressig et al., 1996, 2001; Tyler et al., 2000). Since these KIEs differ considerably, the $\delta D(H_2O)$ distribution in the middle atmosphere is expected to be determined by the partitioning of the different CH_4 oxidation reactions.

(ii) Re-cycling of oxygen atoms between H_2O and the oxygen reservoir gases O_2 and O_3 via HO_x and NO_x species and oxygen isotope exchange reactions. Besides net H_2O formation due to CH_4 oxidation, continuous loss of H_2O and reformation of H_2O lead to an extensive turnover of oxygen atoms between oxygen containing trace gases. This process recycles much more H_2O molecules than are net produced by the oxidation of CH_4 (see Fig. 5). Though a zero-cycle with respect to the H_2O mass, it strongly influences the oxygen isotope composition of H_2O. This process is expected to dominate the MIF oxygen isotope signal from O_3 to H_2O. Further processes to be considered are a few oxygen isotope exchange reactions such as between OH and H_2O and NO_2 and H_2O.

A crucial and exciting point is that more than 99% of all oxygen atoms that end up in H_2O in the middle atmosphere stem from the hydroxyl radical OH. Hence, $\delta^{17}O(H_2O)$ and $\delta^{18}O(H_2O)$ data provide information about the oxygen isotope composition of OH, and by considering $\Delta^{17}O(H_2O)$ about the affection of MIF enriched O_3 upon OH_x and via OH_x upon many other oxygen containing trace gases in the middle atmosphere. This MIF transfer from O_3 to oxygen-containing radicals was first studied by Lyons (2001).

4 Model description

Our 1-D model encompasses 65 boxes from 15 to 80 km, each 1 km high. Temperature and pressure profiles are set according to the U.S. Standard Atmosphere (1976). Vertical transport is parameterised by eddy diffusion coefficients K_z, below 29 km using the "National Academy of Science (1976)" profile, from 29 km to 50 km using the "Hunten" profile, both depicted by Massie and Hunten (1981), and above 50 km employing the profile given by Froidevaux and Yung (1982).

4.1 Peculiarities in modelling isotope ratios

The concept of chemical families frequently applied in atmospheric chemistry models mostly fails if isotopologues are considered. For instance, the reaction chain of $CO+OH\rightarrow CO_2+H$ followed by $H+O_2+M\rightarrow HO_2+M$ converts OH to HO_2, which conserves the sum of HO_x=OH+HO_2. The oxygen atom of the initial OH, however, is incorporated in CO_2 and thus leaves the HO_x family. A new OH bond is formed, which has the oxygen isotope composition of O_2.

The following peculiarities also have to be taken into account:

(i) Kinetic isotope fractionation factors that account for the mostly slower reaction rate of the isotopically substituted molecule compared to the most abundant isotopologue.

(ii) Isotope exchange reactions such as the fast O exchange between O_2 and $O(^3P)$ (Kaye and Strobel, 1983). They modify isotope ratios but not the concentration of the participating compounds.

(iii) When including isotopologues and isotopomers that contain two or more atoms of the same element at non-equivalent positions such as O_3 or HO_2, the individual isotopomers have to be considered separately, e.g. the OQO and OOQ or HQO and HOQ (with Q substituting for ^{17}O and ^{18}O).

4.2 Trace gas chemistry

Due to negligible cloud formation in the middle atmosphere, our model is restricted to gas phase chemistry. If not cited differently, all reaction rates are taken from JPL (2003). Initially, all reactions involved in H_2O chemistry and isotope exchange with other gases were assessed carefully for all altitudes covered by the model. The reactions finally used (Tables 1 and 2) always account for more than 95% of the local chemical turnover of H_2O and its isotopologues at a given altitude.

Water vapour is formed due to H-abstraction by OH, i.e. $XH_i+OH\rightarrow XH_{i-1}+H_2O$, where XH_i is CH_4 (Reaction R1), CH_2O (R8), HO_2 (R16), HCl (R21), H_2 (R26), or HNO_3 (R29). The major sinks of middle atmospheric H_2O are the reaction with $O(^1D)$ (R30) and photolysis at wavelength below 200 nm (R31).

Furthermore, all reactions that are necessary to maintain the overall budget of O- and H-atoms balanced are included. To this end a complete methane destruction scheme (LeTexier et al., 1988) and all relevant reactions affecting the HO_x-family (Burnett and Burnett, 1995) are considered.

The concentrations and the isotopic compositions of H_2O, OH, HO_2, H, H_2, CH_4, CH_3, CH_2O, HCO, HNO_3, and HCl are explicitly calculated by the model.

4.3 Isotope chemistry

Integration of isotopologues renders the model complex, as shown for the initial steps of the major methane destruction reactions (Table 3).

Only for a few of the reactions listed in Table 1 the isotope fractionation factor KIE=k/k' is known, with k' being the rate constant for the isotopically substituted species. All KIEs that have been measured in the laboratory are implemented in the model (Table 5), expressed in the form:

$$\mathrm{KIE} = A \cdot \exp(E/T) \quad (2)$$

Table 1. Considered gas phase reactions.

No	reaction	rate [a] A	rate [a] E	br, n [b]
(R1)	$CH_4+OH \longrightarrow CH_3+H2O$		Table 3	
(R2)	$CH_4+O(^1D) \longrightarrow ...$		Table 3	
(R3)	$CH_4+Cl \longrightarrow CH_3+HCl$		Table 3	
(R4)	$CH_4+\gamma \longrightarrow CH_3+H$		Table 3	
(R5)	$CH_3 + O_2 + M \longrightarrow CH_3O_2 + M$		Table 2	
(R6)	$CH_3O_2+NO \longrightarrow CH_3O+NO_2$	2.8(−12)	−300	
(R7)	$CH_3O+O_2 \longrightarrow CH_2O+HO_2$	3.9(−14)	900	
(R8)	$CH_2O+OH \longrightarrow CHO+H_2O$	1.0(-11)	0	
(R9)	$CH_2O+\gamma \longrightarrow CHO+H/CO+H_2$	altitude dependent		
(R10)	$CH_2O+O(^3P) \longrightarrow CHO+OH$	3.4(−10)	1600	
(R11)	$CH_2O+Cl \longrightarrow CHO+HCl$	8.1(−11)	30	
(R12)	$HCO+O_2 \longrightarrow CO+HO_2$	3.5(−12)	−140	
(R13)	$H+O_2+M \longrightarrow HO_2+M$		Table 2	
(R14)	$H+O_3 \longrightarrow OH+O_2$	1.4(−10)	470	
(R15)[a]	$H+HO_2 \longrightarrow 2OH$	8.1(−11)	0	0.87
(R15)[b]	$H+HO_2 \longrightarrow H_2O+O_2$	8.1(−11)	0	0.09
(R15)[c]	$H+HO_2 \longrightarrow H_2O+O(^3P)$	8.1(−11)	0	0.02
(R16)	$OH+HO_2 \longrightarrow H_2O+O_2$	4.8(−11)	−250	
(R17)	$OH+O_3 \longrightarrow HO_2+O_2$	1.6(−12)	940	
(R18)	$OH+O(^3P) \longrightarrow H+O_2$	2.2(−11)	−120	
(R19)	$OH+OH \longrightarrow H_2O+O(^3P)$	4.2(−12)	240	
(R20)	$OH+NO_2+M \longrightarrow HNO_3+M$		Table 2	
(R21)	$HCl+OH \longrightarrow H_2O+Cl$	2.6(−12)	350	
(R22)	$CO+OH \longrightarrow CO_2+H$	1.5(−13)	0	
(R23)	$HO_2+NO \longrightarrow OH+NO_2$	3.5(−12)	−250	
(R24)	$HO_2+O(^3P) \longrightarrow OH+O_2$	3.0(−11)	−200	
(R25)	$HO_2+O_3 \longrightarrow OH+2{\cdot}O_2$	1.1(−14)	500	
(R26)	$H_2+OH \longrightarrow H_2O+H$	5.5(−12)	2000	
(R27)	$H_2+O(^1D) \longrightarrow H+OH$	1.1(−10)	0	
(R28)	$H_2+Cl \longrightarrow H+HCl$	3.7(−11)	2300	
(R29)	$HNO_3+OH \longrightarrow H_2O+NO_3$			
(R30)	$H_2O+O(^1D) \longrightarrow 2{\cdot}OH$	2.2(−10)	0	
(R31)[a]	$H_2O+\gamma \longrightarrow H+OH$, γ=121.6 nm	5.25(−6)	−4.4(−19)	0.917
(R31)[b]	$H_2O+\gamma \longrightarrow H+OH$, γ>130 nm	1.20(−6)	−1.0(−7)	0.35

[a] rate constant $k(T)$=A· exp[−(E·K/T)] in $cm^3\,s^{-1}$
photolysis rate j (z)=A· exp[E·L(z)^n] in s^{-1}, with L(z): number of molecules cm^{-2} above altitude z.
[b] br: branching rate, n: exponent in j (z)

For some KIEs no temperature dependence is known and thus is set constant. For the reactions for which the KIE has not been explicitly measured, KIE is set to $(\mu'/\mu)^{1/2}$, with $\mu=m_1{\cdot}m_2/(m_1+m_2)$ being the reduced mass of the reactants of mass m_1 and m_2. This accounts for the fact that the rate constant of a certain reaction does not only depend on the reactivity of the reactants, but also on their collision frequency and thus thermal speed.

Additionally, the known oxygen exchange reactions were included (Table 5).

4.4 Trace gas parameter profiles

Fixed, globally, seasonally and diurnally averaged profiles are used for the trace gases O_3, $O(^1D)$, NO, NO_2, and Cl. These were derived from a simulation of the Mainz photochemical 2-D model (Grooß, 1996), as an annually and diurnally averaged profile of the HNO_3 photolysis frequency.

Table 2. Termolecular reactions.

No.	Reaction	k_0^{300} [a]	n	k_∞^{300} [b]	m
(5)	$CH_3+O_2+M\longrightarrow CH_3O_2+M$	4.5×10^{-31}	3.0	1.8×10^{-12}	1.7
(13)	$H+O_2+M\longrightarrow HO_2+M$	5.7×10^{-32}	1.6	7.5×10^{-11}	0.0
(20)	$OH+NO_2+M\longrightarrow HNO_3+M$	2.5×10^{-30}	4.4	1.6×10^{-11}	1.7

[a] $k_0(T)=k_0^{300}\cdot(\frac{T}{300})^{-n}$
[b] $k_\infty(T)=k_\infty^{300}\cdot(\frac{T}{300})^{-m}$
rate constant $k(M,T)=(\frac{k_0(t)[M]}{1+(k_0(T)[M]/k_\infty(T))})\cdot0.6^{(1+[\log_{10}(k_0(t)[M]/k_\infty(T))]^2)^{-1}}$
$[M]$ being the number concentrations of air molecules and T the temperature.

Table 3. Detailed description of the initial methane destruction reactions.

No	reaction	rate A	rate E	branching ratio	fractionation factor
(1)	$CH_4+OH\longrightarrow CH_3+H_2O$	2.45 (−12)	1775	1	1
	$CH_4+{}^{17}OH\longrightarrow CH_3+H_2{}^{17}O$	2.45 (−12)	1775	1	0.986
	$CH_4+{}^{18}OH\longrightarrow CH_3+H_2{}^{18}O$	2.45 (−12)	1775	1	0.973
	$CH_4+OD\longrightarrow CH_3+HDO$	2.45 (−12)	1775	1	Table 4
	$CH_3D+OH\longrightarrow CH_2D+H_2O$	3.5 (−12)	1950	0.75	0.985
	$CH_3D+OH\longrightarrow CH_3+HDO$	3.5 (−12)	1950	0.25	0.985
	$CH_3D+OD\longrightarrow CH_2D+HDO$	3.5 (−12)	1950	0.75	0.971
	$CH_3D+OD\longrightarrow CH_3+D_2O$	3.5 (−12)	1950	0.25	0.971
(2)	$CH_4+O(^1D)\longrightarrow CH_3+OH$	1.5 (−10)	0	0.75	1
	$CH_4+{}^{17}O(^1D)\longrightarrow CH_3+{}^{17}OH$	1.5 (−10)	0	0.75	0.985
	$CH_4+{}^{18}O(^1D)\longrightarrow CH_3+{}^{18}OH$	1.5 (−10)	0	0.75	0.972
	$CH_4+O(^1D)\longrightarrow CH_3O+H$	1.5 (−10)	0	0.20	1
	$CH_4+{}^{17}O(^1D)\longrightarrow CH_3{}^{17}O+H$	1.5 (−10)	0	0.20	0.985
	$CH_4+{}^{18}O(^1D)\longrightarrow CH_3{}^{18}O+H$	1.5 (−10)	0	0.20	0.972
	$CH_4+O(^1D)\longrightarrow CH_2O+H_2$	1.5 (−10)	0	0.05	1
	$CH_4+{}^{17}O(^1D)\longrightarrow CH_2{}^{17}O+H_2$	1.5 (−10)	0	0.05	0.985
	$CH_4+{}^{18}O(^1D)\longrightarrow CH_2{}^{18}O+H_2$	1.5 (−10)	0	0.05	0.972
	$CH_3D+O(^1D)\longrightarrow CH_3+OD$	1.5 (−10)	0	0.75·0.70	Table 4
	$CH_3D+O(^1D)\longrightarrow CH_2D+OH$	1.5 (−10)	0	0.25·0.70	Table 4
	$CH_3D+O(^1D)\longrightarrow CH_2DO+H$	1.5 (−10)	0	0.75·0.20	Table 4
	$CH_3D+O(^1D)\longrightarrow CH_3O+D$	1.5 (−10)	0	0.25·0.20	Table 4
	$CH_3D+O(^1D)\longrightarrow CHDO+H_2$	1.5 (−10)	0	0.75·0.05	Table 4
	$CH_3D+O(^1D)\longrightarrow CH_2O+HD$	1.5 (−10)	0	0.25·0.05	Table 4
(3)	$CH_4+Cl\longrightarrow CH_3+HCl$	1.1 (−11)	1400	1	1
	$CH_3D+Cl\longrightarrow CH_3+DCl$	1.1 (−11)	1400	0.25	Table 4
	$CH_3D+Cl\longrightarrow CH_2D+HCl$	1.1 (−11)	1400	0.75	Table 4
(4)	$CH_4+\gamma\longrightarrow CH_3+H$	5.5 (−6)	−4.4(−19)	1	n=0.917 [a]
	$CH_3D+\gamma\longrightarrow CH_3+D$	5.5 (−6)	−4.4(−19)	0.25	n=0.917 [a]
	$CH_3D+\gamma\longrightarrow CH_2D+H$	5.5 (−6)	−4.4(−19)	0.75	n=0.917 [a]

[a] Brasseur and Solomon (1986), with photolysis rate $j(z)=A\cdot\exp[E\cdot L(z)^n]$ in s^{-1}, L(z) being the number of molecules per cm^2 above altitude z.

4.5 Isotope parameter profiles of $O(^3P)$, O_3, $O(^1D)$, and NO

The oxygen isotope compositions assumed for O_2, $O(^3P)$, O_3, and $O(^1D)$ are indicated in Fig. 1 together with the calculated isotope profiles for NO, OH, and HO_2.

The isotope composition of
(i) O_2 is $\delta^{17}O(O_2)$ = 11.78‰ and $\delta^{18}O(O_2)$=22.96‰ (Luz et al., 1999; Coplen et al., 2002),
(ii) $O(^3P)$ is controlled by the rapid exchange reaction with O_2 (Kaye and Strobel, 1983), which shows significant

Table 4. Considered fractionation factors, defined as KIE(T)=KIE(0)· exp(B/T).

No	reaction	KIE(0)	B[a]	KIE(300K)	reference
(1)	$CH_3D+OH \longrightarrow CH_2D+H_2O$	0.605	215.00	1.239	Gierczak et al. (1997)
(1)	$CH_4+OD \longrightarrow CH_3+HDO$	1.120	−55.00	0.932	Gierczak et al. (1997)
(2)	$CH_3D+O(^1D) \longrightarrow CH_3+OD$	1.060	0.00	1.060	Saueressig et al. (2001)
(3)	$CH_3D+Cl \longrightarrow CH_3+DCl$	1.278	51.31	1.516	Saueressig et al. (1996)
(8)	$CHDO+OH \longrightarrow HCO+HDO$	0.7812	0.00	0.781	Feilberg et al. (2004)
(8)	$CH_2Q+OH \longrightarrow HCO+H_2Q$	1.0341	0.00	1.034	Feilberg et al. (2004)
(11)	$CHDO+Cl \longrightarrow HCO+DCl$	0.8326	0.00	0.833	Feilberg et al. (2004)
(11)	$CH_2Q+Cl \longrightarrow HCQ+DCl$	0.9259	0.00	0.926	Feilberg et al. (2004)
(26)	$HD+OH \longrightarrow HDO+H$	1.100	130.00	1.697	JPL (2003)
(27)	$HD+O(^1D) \longrightarrow H+OD$	1.130	0.00	1.130	Talukdar and Ravishankara (1996)

[a] if B = 0, no temperature dependency has been measured so far.

Table 5. Considered oxygen isotope exchange reactions.

No	reaction	Rate		reference
		A	E	
(32)	$QH+NO \rightleftharpoons OH+NQ$	1.8(−11)	0	Dubey et al. (1997)
(33)	$QH+NO_2 \rightleftharpoons OH+NOQ$	1.0(−11)	0	Greenblatt and Howard (1989)
(34)	$QH+H_2O \rightleftharpoons OH+H_2Q$	1.6(−13)	2100	Greenblatt and Howard (1989)
(35)	$HOQ+OH \rightleftharpoons HO_2+QH$	1.7(−11)	−400	Dransfeld and Wagner (1987)
(36)	$Q+O_2 \rightleftharpoons OQ+O$			see Sect. 4.5
(37)	$Q+NO \rightleftharpoons O+NQ$			see Sect. 4.5
(38)	$NOQ+H_2O \rightleftharpoons NO_2+H_2Q$	2.3(−13)	2100	Jaffe and Klein (1966)
(39)	$QH+O_2 \rightleftharpoons OH+OQ$	<1(−17)	0	Greenblatt and Howard (1989)
(40)	$HOQ+O_2 \rightleftharpoons HO_2+OQ$	<3(−17)	0	Sinha et al. (1987)
(41)	$NOQ+O_2 \rightleftharpoons NO_2+OQ$	<1(−24)	0	Sharma et al. (1970)

fractionation and leads to $\delta^{17}O(O(^3P))=-27.58‰$ and $\delta^{18}O(O(^3P))=-55.30‰$ (Johnston et al., 2000).
(iii) O_3 was set to be solely dependent on temperature, because all laboratory data indicate negligible pressure dependence below 100 hPa and because it appears that all reliable atmospheric data agree with the enrichments determined in laboratory studies (Johnson et al., 2000; Mauersberger et al., 2001). The (consistent) laboratory data by Thiemens and Jackson (1988, 1990), Morton et al. (1990), and (Günther et al., 1999) are implemented under the assumption that 80% of the isotope enrichment of O_3 is carried by the asymmetric QOO (Anderson et al., 1989; Janssen et al., 1999; Mauersberger et al., 1999).

$Q(^1D)$ is derived from the isotope enrichment in O_3 under the following further assumptions: (i) during the photolysis of O_3 only the terminal oxygen atoms form $O(^1D)$, (ii) there is negligible fractionation during the photolysis of O_3 (Wen and Thiemens, 1993), and (iii) mass-dependent collision rates during subsequent quenching of $O(^1D)$ on N_2 and O_2 to the ground state $O(^3P)$ lead to additional isotope enrichment of 19‰ for $\delta^{17}O$ and 36‰ for $\delta^{18}O$ in $O(^1D)$ (calculated by using the formula given in Sect. 4.3).

The oxygen isotope composition of middle atmospheric NO_x is not controlled by its main source, i.e. oxidation of N_2O by $O(^1D)$, but by O exchange between O_x and NO_x:

$$NO + O_3 \rightarrow NO_2 + O_2 \quad \text{(NO-1)}$$

$$NO_2 + O(^3P) \rightarrow NO + O_2 \quad \text{(NO-2)}$$

and the fast O-exchange reactions:

$$NO + Q(^3P) \rightleftharpoons NQ + O(^3P) \quad \text{(NO-3)}$$

$$NO + QH \rightleftharpoons NQ + OH \quad \text{(NO-4)}$$

Indeed, because of the rapid photochemical cycling less than 0.5% of all O atoms in NO stem from the oxidation of N_2O by $O(^1D)$ over the entire altitude range considered. Hence, the isotopic composition of N_2O that is known to carry a small degree of MIF into the stratosphere (Cliff and Thiemens, 1997; Cliff et al., 1999; Röckmann et al., 2001a; Röckmann et al., 2001b; Kaiser and Röckmann, 2005) does not need to be considered. Using a sub-model, the O isotope ($\delta^{17}O$, $\delta^{18}O$) parameter profile of NO is derived by calculating the source partitioning of the reactions NO-1 to NO-4. The inferred enrichments in NO and NO_2 (Fig. 1) in the

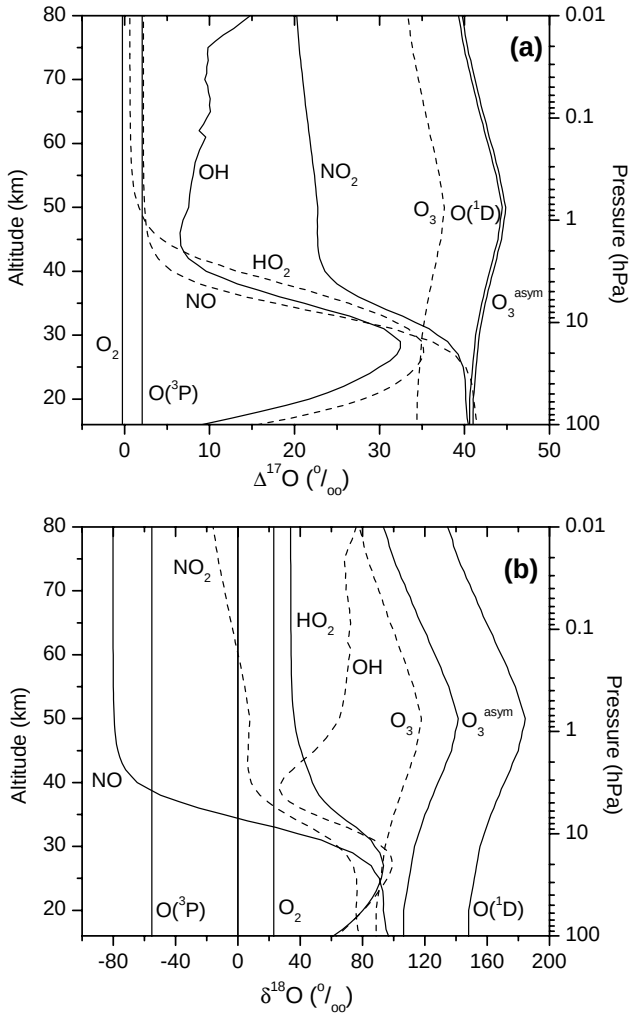

Fig. 1. Vertical profile of $\Delta^{17}O$ (graph a) and $\delta^{18}O$ (graph b) assumed for O_2, $O(^3P)$, O_3, asymmetric O_3, and $O(^1D)$, and calculated for NO, OH and HO_2 (without considering the isotope exchange reactions R39 and R40).

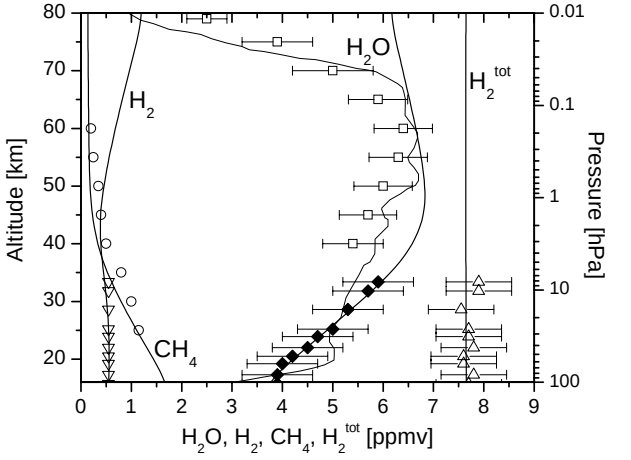

Fig. 2. Calculated vertical profiles of H_2O, CH_4, H_2, and H_2^{tot} compared to measurements of H_2O: balloon-borne in situ Lyman-α hygrometer data at 43° N (black diamonds) (Zöger et al., 1999), ATMOS data (light squares) (Michelsen et al., 2002), and HALOE data (line) (Nedoluha et al., 1998); CH_4, H_2: cryogenic collection and subsequent laboratory analysis at 43° N (Zöger et al., 1999), and H_2^{tot}: (Zöger et al., 1999).

lower stratosphere (which is due to the O exchange with O_3, reactions NO-1 and NO-2) is only about half the ones calculated by Lyons (2001), explanation in Sect. 7. Because of the dominance of NO-3, the oxygen isotopic composition of NO in the mesosphere is similar to the one of $O(^3P)$.

4.6 Boundary conditions

At the lower model boundary, i.e. the tropopause, fixed trace gas and isotope mixing ratios are set as follows: $[H_2O]$=3.70 μmol/mol. $\delta D(H_2O)$=−660‰ and $\delta^{18}O(H_2O)$=−128‰ (Moyer et al., 1996; Johnson et al., 2001, Kuang et al., 2003, McCarthy et al., 2004). $\Delta^{17}O(H_2O)$ is set to 0‰ (as no process is known in the troposphere, which could cause MIF in H_2O), so that $\delta^{17}O(H_2O)$ is –69.76‰ (in agreement with –(84 ± 31)‰ observed by Johnson et al., 2001). $[CH_4]$=1.70 μmol/mol. $\delta D(CH_4)$=−86‰ (Quay et al., 1999). $[H_2]$=0.55 μmol/mol (Zöger et al., 1999). $\delta D(H_2)$=130‰ (Friedman and Scholz, 1974; Rahn et al., 2003; Rhee et al., 2006). The flux of all considered species across the upper boundary (80 km) is set to zero.

5 Model results and comparison with observations

The model results presented in this section constitute the "base run" where the badly quantified isotope exchange reactions (R38) to (R41) (Table 5) are omitted. The influence of these badly quantified reactions is assessed in Sect. 6.5.

5.1 Vertical trace gas profiles

In Fig. 2 calculated vertical profiles for H_2O, CH_4, H_2 and the total hydrogen H_2^{tot} are compared with observations. The agreement is good. The difference above 70 km is due to the known strong seasonal variation in this altitude range. For instance, H_2 is expected to vary between 1 ppmv in July and nearly 3 ppmv in January at 70 km altitude (LeTexier et al., 1988).

The destruction of methane in the stratosphere leads to a relevant increase in water vapour. Maximum mixing ratios of 6.5 ppmv are observed at the stratopause. Above 50 km, increasing loss of H_2O due to reaction with OH and above 65 km due to photolysis overcompensates H_2O formation and causes a decline in H_2O and an increase in H_2. The total hydrogen H_2^{tot} stays constant in the middle atmosphere. The weak decrease in the mesosphere comes along with increasing concentrations of atomic hydrogen H.

5.2 Vertical profiles of δD(H_2O), δD(CH_4), and δD(H_2)

The calculated profiles of δD in H_2O, CH_4, and H_2 likewise compare well with observations and the model results obtained by Ridal (2002) for δD(H_2O) (Fig. 3).

Apart from the Arctic profile retrieved by (Stowasser et al., 1999), all available δD(H_2O) observations (Sect. 2) (although somewhat differing in absolute concentrations) show a vertical increase by ∼(150–200)‰ between 20 and 40 km. This vertical δD(H_2O) increase is due to the increasing fraction of H_2O that originates from the oxidation of CH_4 (see Sect. 3). The δD(H_2O) value in the mesosphere, which is higher than the tropopause value by ∼250‰, suggests that ∼60% of the mesospheric H_2O originate from the troposphere and ∼40% stem from the oxidation of CH_4 (see Sect. 6.3).

The δD profiles of CH_4 and H_2 agree well with in-situ sampling and subsequent mass-spectrometric laboratory measurements by Röckmann et al. (2003) and Brass et al. (MPI-K Heidelberg, personal communication).

5.3 Vertical Profiles of δ^{17}O(H_2O) and δ^{18}O(H_2O)

The oxygen isotope ratios in H_2O (Fig. 4) exhibit a vertical profile that is qualitatively similar to that of δD(H_2O). However, for the O isotopologues in addition to new H_2O formation photochemical recycling, that is exchange of oxygen isotopes with O_2 and O_3 via HO_x- and NO_x-species, causes additional intensive turnover of δ^{17}O(H_2O) and δ^{18}O(H_2O). As a consequence, the relative enrichments are even stronger than for δD, and positive values for δ^{17}O and δ^{18}O are reached. Note that both recycled H_2O and newly formed H_2O have the same O isotope signature since both are produced mainly via HO_x (see Sect. 6.4).

The measurements by Dinelli et al. (1991), Guo et al. (1989), Rinsland et al. (1991), and Johnson et al. (2001) are in reasonable agreement with our model results. Consider however the large measurement errors of ±(50–120)‰ which is in the same magnitude as the calculated total vertical increase by 85‰ for δ^{17}O(H_2O) and 150‰ for δ^{18}O(H_2O).

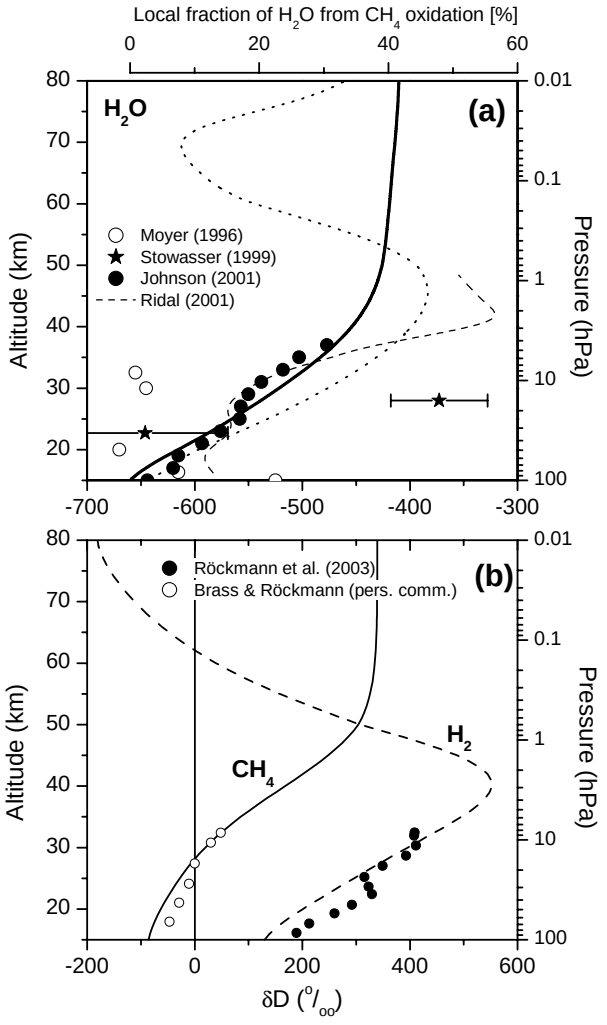

Fig. 3. Calculated vertical profile of δD in H_2O (graph a, thick line), and CH_4 and H_2 (graph b) compared to measurements. **(a)** Dotted line: δD of freshly produced H_2O. Open circles: ATMOS FTIR data of near-global latitudinal coverage (Moyer et al., 1996). Full circles: Smithsonian Astrophysical Observatory's far-infrared data by Johnson et al. (2001a). Stars: Balloon-borne MIPAS data inside the Arctic vortex at 68° N (Stowasser et al., 1999). Dashed line: 1-D model result by Ridal et al. (2001). Upper x-axis indicates the approximate fraction of H_2O from the CH_4 oxidation inferred from the δD(H_2O) value (explanation, see Sect. 6.3). **(b)** Full and open circles: Laboratory mass-spectrometer data of in-situ samples.

6 Discussion

6.1 The budget of middle atmospheric water vapour

Figure 5 exhibits the turnover rates of water vapour in the middle atmosphere. The annual flux of tropospheric water into the stratosphere is set to 788 Mt (Yang and Tung, 1996). In the stratosphere further 63.9 Mt H_2O (and 0.31 Mt H_2) is net produced due to the oxidation of CH_4. The calculated annual CH_4 destruction rate is 30 Mt yr^{-1}. This value is slightly lower than the (40±10) Mt yr^{-1} often reported (Crutzen, 1995; Lelieveld et al., 1998), but agrees with Gettelmann et al. (1998) and exceeds earlier values given by Crutzen (1991) and Khalil et al. (1993). The calculated ratios between H_2O and H_2 production and CH_4 loss for the entire middle atmosphere are:

$$\frac{P(H_2O)}{L(CH_4)} = 1.90 \quad \text{and} \quad \frac{P(H_2)}{L(CH_4)} = 0.10 \qquad (5)$$

Using a coupled chemistry/dynamical model (LeTexier et al., 1988) derived $P(H_2O)/L(CH_4)$=1.6 which is in agreement with satellite observations by Hanson and Robinson (1989). More recent in situ measurements indicated higher values of 1.94±0.27 (Dessler et al., 1994), 1.82±0.21 (Engel et al.,

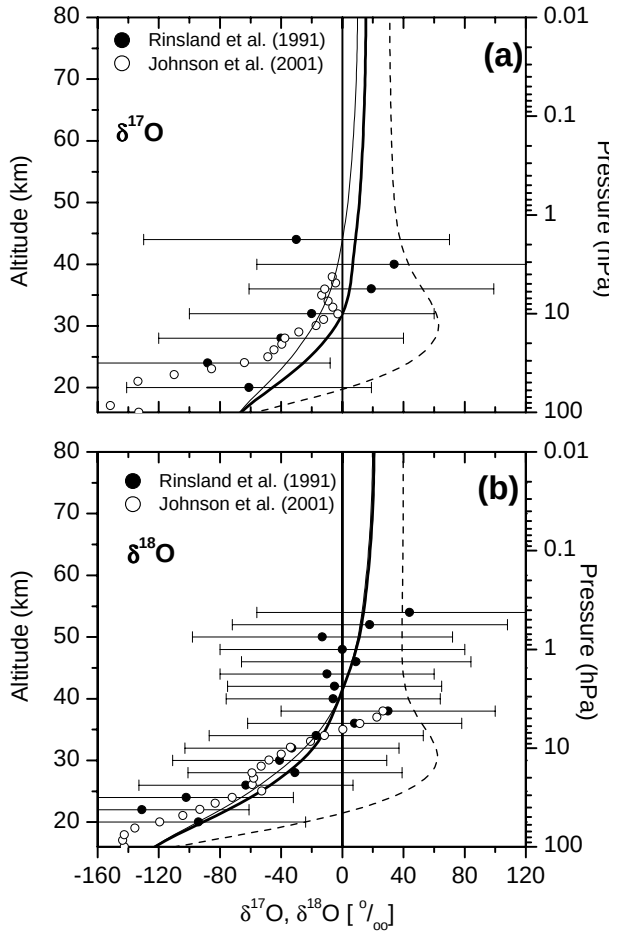

Fig. 4. Calculated vertical profiles of $\delta^{17}O(H_2O)$ (graph a) and $\delta^{18}O(H_2O)$ (graph b) compared to ATMOS Spacelab 3 infrared solar spectra near 30° N (Rinsland et al., 1991) and FTIR balloon-borne data at 33° and 68° N (Johnson et al., 2001). Thick straight lines: base run. Dashed lines: Oxygen exchange reaction (R38) ($NOQ+H_2O \rightleftharpoons NO_2+H_2Q$) is considered at its estimated upper limit. Thin straight lines: Oxygen exchange reactions (R39) ($QH+O_2 \rightleftharpoons OH+OQ$) and (R40) ($HOQ+O_2 \rightleftharpoons HO_2+OQ$) are considered at their estimated upper limits.

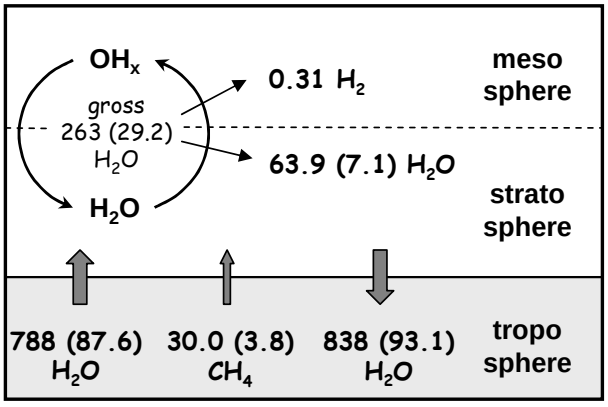

Fig. 5. Middle atmospheric budget of H_2O. Numbers are mass fluxes in $Mt\,yr^{-1}$. Numbers in parenthesis are fluxes of H_2 in $Mt\,yr^{-1}$. The H_2O flux into the stratosphere is adopted from Yang and Tung (1996), other numbers are model results.

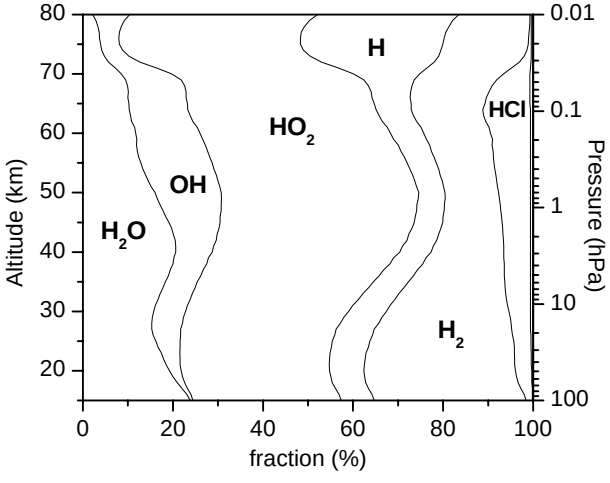

Fig. 6. Calculated percentage fraction of hydrogen atoms that are transferred during the initial oxidation reaction of CH_4 either to H_2O, OH, OH_2, H, H_2, or HCl.

1996), 1.973±0.003 (Hurst et al., 1999), and 1.975±0.030 (Zöger et al., 1999), which are in reasonable agreement with our model results.

Interestingly, although each CH_4 molecule finally results in the formation of almost two H_2O molecules (Eq. 5), most hydrogen atoms in CH_4 make the detour via other gases to H_2O, as demonstrated in Fig. 6. Only ∼15% of all H_2O molecules are formed directly from one of the four H atoms of CH_4 or intermediate products in the CH_4 destruction chain (such as formaldehyde, CH_2O), i.e., are produced via reactions:

$$CH_4 + OH \rightarrow CH_3 + H_2O \quad \text{(R1)}$$

$$CH_2O + OH \rightarrow CHO + H_2O \quad \text{(R8)}$$

The other ∼85% of the H atoms in CH_4 are incorporated first in OH, HO_2, H_2, H, or HCl, before ending up in H_2O. This detour the H atoms take from CH_4 to H_2O certainly affects not only the isotope composition of the final product H_2O, but also that of the intermediate species (OH, HO_2, HCO, H_2, H, HCl etc.).

Figure 7 presents the vertical profile of H_2O production $P(H_2O)$ and loss $L(H_2O)$. Both $P(H_2O)$ (dominated by the reaction $OH+HO_2 \rightarrow H_2O+O_2$ – Kaye, 1990) and $L(H_2O)$ (more than 99% of which are due to the reaction of $H_2O+O(^1D) \rightarrow 2\,OH$) peak at ∼38 km altitude. The net rate, $P(H_2O) - L(H_2O)$, amounts to ∼27% of $P(H_2O)$ only. It shows a wide maximum centred at 35–40 km, that is ∼5 km above the maximum of the CH_4 loss rate (for better comparison $2\times L(CH_4)$ is shown, dotted line). This again emphasises that during the oxidation of CH_4 most H atoms are first

incorporated in intermediate species (where the longer lived ones H_2, HCl, and HNO_3 experience spatial redistribution) before ending up in H_2O, and that a considerable turnover of H_2O molecules occurs in the middle atmosphere which significantly exceeds the net production of H_2O.

6.2 The chemical lifetimes of H_2O, $\delta D(H_2O)$, $\delta^{17}O(H_2O)$, and $\delta^{18}O(H_2O)$

Division of the local H_2O concentration by the local H_2O loss rate $L(H_2O)$ yields the chemical lifetime of H_2O, $\tau(H_2O)$, at a certain altitude (Fig. 7b). As the same reactions control the loss of HDO molecules, the chemical lifetime of HDO, $\tau(HDO)$, is identical with $\tau(H_2O)$. In the entire middle atmosphere $\tau(H_2O)$ or $\tau(HDO)$, respectively, (like $\tau(CH_4)$) exceeds the vertical transport time scale H^2/K_z (H being the local scale height and K_z the vertical eddy diffusion coefficient). That is, neither H_2O nor HDO is in photochemical equilibrium in the middle atmosphere. Only between 35 and 50 km altitude, the transport time scale almost compares with the photochemical lifetime of H_2O (and HDO), in agreement with (LeTexier et al., 1988). Below 35 km, $\tau(H_2O)$ and $\tau(HDO)$ exceeds ∼5 years.

Consider moreover, that the influence of in-situ H_2O production due to CH_4 oxidation on $\delta D(H_2O)$ is small below ∼30 km, too. This can be seen in Fig. 7a, when the net H_2O production (black line) displayed in molecules $cm^{-3}\,s^{-1}$ is divided by the pressure, which gives the H_2O production in $ppmv\,s^{-1}$. This number peaks at 45 km and is small below ∼30 km.

The latter conclusion and the long chemical lifetime implies that below 30–35 km the H_2O mixing ratio as well as its δD value is largely dominated by transport, i.e. by vertical transport for the present 1-D model. Thus, between the tropopause and 30-35 km the H_2O mixing ratio and its δD value is determined by (vertical) mixing of two reservoirs, the one at the tropopause which is controlled by (physical) fractionation processes in the troposphere, and the second above 30–35 km which is determined by the dominant H_2O loss reaction (R30).

For the oxygen isotopologues $\delta^{17}O(H_2O)$ and $\delta^{18}O(H_2O)$, additional oxygen exchange of H_2O with other gases (Reactions R34 and R38) causes somewhat shorter lifetimes of the $\delta^{17}O$ and $\delta^{18}O$ signature of the stratospheric water vapour. Moreover, the vital recycling of water (via HO_x species) only weakly affects the $\delta D(H_2O)$ value, because H_2O is the major hydrogen reservoir in the mesosphere. This is not the case for $\delta^{17}O(H_2O)$ and $\delta^{18}O(H_2O)$, where the many intermediate species involved in the H_2O recycling process exchange oxygen atoms with the other major oxygen "reservoirs" O_2 and O_3.

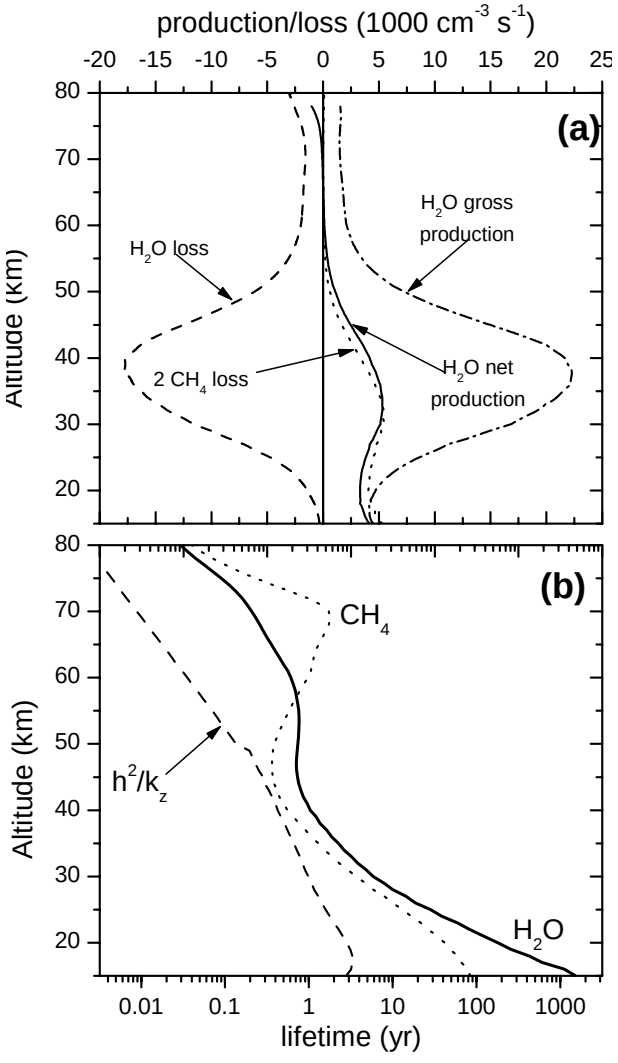

Fig. 7. **(a)** calculated vertical profiles of H_2O production and loss rates in the middle atmosphere. For comparison, the double CH_4 loss rate is shown (as almost two H_2O molecules are net produced for each oxidised CH_4 molecule, see Eq. 5). **(b)** comparison of the photochemical lifetime of H_2O and CH_4 with the transport time scale (h^2/k_z, with h: atmospheric scale height and k_z: vertical eddy diffusion coefficient).

6.3 $\delta D(H_2O)$ as tracer for CH_4 oxidation

Tropospheric H_2O is imported into the stratosphere with $\delta D(H_2O) \approx -660‰$ (Moyer et al., 1996; Johnson et al., 2001; Kuang et al., 2003; McCarthy et al., 2004). Tropospheric CH_4 carries much higher δD values of roughly −86‰ (Quay et al., 1999) into the stratosphere. The vertically increasing contribution of H_2O produced by the oxidation of CH_4 is described by the upper x-axis of Fig. 3. It shows the local fraction of H_2O from CH_4 oxidation $\mathcal{F}$, that is the ratio between the difference of the local $\delta D(H_2O)$ value to the tropopause value (–660‰) and the difference of the $\delta D(H_2O)$ from the

CH_4 oxidation (set to –86‰) and the $\delta D(H_2O)$ tropopause value, i.e.,

$$\mathcal{F} = \frac{\delta D(H_2O) - (-660‰)}{-86‰ - (-660‰)} \quad (6)$$

Figure 3 indicates that ∼40% of the water vapour present above 40 km originate from the oxidation of CH_4. For simplicity, we have set $\delta D(CH_4)$ constant, although in reality it varies with altitude (Fig. 3b). The influence of this simplification is surprisingly weak. This has two reasons. First, the contributions of the three main CH_4 loss reactions (R1–R3) are comparable throughout the middle and upper stratosphere (where the major CH_4 loss occurs). Second, due to the long chemical lifetime of H_2O (and HDO), spatial redistribution smears out the anyway weak vertically changing $\delta D(H_2O)$ source signature.

Unfortunately, this fact also documents that the $\delta D(H_2O)$ value does not constitute a sensitive measure for quantifying the partitioning of the different CH_4 loss reaction chains, contrary to its initial assumption.

Another surprising feature is that both, the δD value of the source molecule CH_4 and the one of the end product H_2O increase with altitude (Fig. 3), although mass conservation for δD at a first glance suggests the opposite behaviour. In all methane oxidation reactions the most abundant CH_4 reacts faster than the isotopically substituted CH_3D (Sect. 3). Hence, the remaining CH_4 is continuously enriched in D/H with altitude. The D/H ratio of the freshly formed H_2O is certainly much lower (dotted line) but is still higher than the D/H ratio of the H_2O lofted from below. Thus, both the δD value of CH_4 and of freshly produced H_2O increases with altitude. Note that for an isotope mass balance the δ values must be multiplied with the concentrations. Here, the concentration of the "D-richer" source CH_4 decreases and the concentration of the D-depleted product H_2O increases. Thus, mass balance is achieved although both δ values increase.

6.4 $\delta^{17}O(H_2O)$ and $\delta^{18}O(H_2O)$ as tracer for transport and chemistry

As outlined in Sect. 3, the oxygen isotope signature of middle atmospheric water vapour is determined by the partitioning of four oxygen isotope sources: (1) mass-dependently fractionated (MDF) H_2O imported from the troposphere, (2) mass-independently fractionated (MIF) H_2O formed as a final product of the oxidation of CH_4, (3) MIF carrying H_2O from the recycling of H_2O via the HO_x family and (4) oxygen atom exchange between H_2O and other gases.

The $\delta^{17}O$ and $\delta^{18}O$ values of source (1), i.e. of H_2O imported from the troposphere, are about –67‰ and –128‰, respectively (see Sect. 4.6). The δO values of water produced by the isotope sources (2) to (4) are controlled by the respective educt molecules and the kinetic isotope fractionation factor KIE of the relevant reaction. As outlined by Kaye (1990) and confirmed by our calculations, more than 99% of all H_2O molecules generated in the middle atmosphere are due to hydrogen abstraction reactions by OH. Thus, the isotope sources (2) and (3) will show the O isotope signature of OH at the respective altitude. H_2O itself undergoes oxygen isotope exchange (i.e. isotope source 4) with OH (R34) and NO_2 (R41, Table 5). Reaction (R34) is too slow to significantly affect the isotope composition of H_2O. The rate constant of Reaction (R38) was not quantified yet; its potentially considerable impact is addressed in Sect. 6.5.

In conclusion, the modification of the oxygen isotope composition of middle atmospheric H_2O is controlled by the oxygen isotope composition of OH. For this reason, the oxygen isotope signature of the different OH sources is studied next. Reaction chains where OH is converted into HO_2 and back into OH without breaking the initial OH bond constitute a zero cycle with respect to the oxygen isotopic composition. Thus, only reactions forming new OH bonds need to be considered.

6.4.1 The formation of new OH bonds

The influence of the most important reactions forming new OH bonds are displayed in Fig. 8a. Four classes of reactions, distinguished by the O isotope signal transferred, form new OH_x bonds:

(i) HO_x that receives the oxygen isotope signature from molecular oxygen via

$$CH_3O + O_2 \rightarrow HO_2 + CH_2O \quad (R7)$$

$$HCO + O_2 \rightarrow HO_2 + CO \quad (R12)$$

$$H + O_2 + M \rightarrow HO_2 + M \quad (R13)$$

Reactions (R7) and (R12) are part of the CH_4 oxidation chain and only play a role below 40 km. Reaction (R13) clearly dominates the formation of new OH bonds in the mesosphere. In addition, oxygen isotope exchange between OH_x and O_2 may occur (Reactions R39 and R40) the influence of which are discussed in Sect. 6.5.

(ii) HO_x that receives the oxygen isotope signature from MIF carrying ozone via

$$H + O_3 \rightarrow OH + O_2 \quad (R14)$$

which is important above 40 km only. Although O_3 also influences the isotope composition of HO_2 via $OH+O_3 \rightarrow HO_2+O_2$, new OH bonds are not formed. The reason is that the oxygen atom that OH receives from O_3 is lost again, simply because HO_2 is an asymmetric molecule (H–O–O).

(iii) HO_x that receives the oxygen signature from MIF carrying $O(^1D)$ and, in the case of Reaction (R30), from H_2O:

$$CH_4 + O(^1D) \rightarrow OH + CH_3 \quad (R2)$$

Table 6. Percentage origin of oxygen isotopes of freshly produced H_2O averaged over stratosphere and mesosphere.

Oxygen Species	Isotope Source isotope signature	base run stratosph.	base run mesosph.	considering R39–R41 stratosph.	considering R39–R41 mesosph.	considering R38 stratosph.	considering R38 mesosph.
O_2	MDF[a]	79.5	74.6	98.1	77.5	70.0	74.6
O_3	MIF[b]	16.5	25.3	1.5	22.4	26.6	25.3
$O(^1D)$	MIF[b]	2.1	0.0	0.2	0.0	1.8	0.0
others		1.9	0.1	0.2	0.1	1.6	0.1

[a] MDF = mass-dependently fractionated
[b] MIF = mass-independently fractionated

$$H_2 + O(^1D) \rightarrow OH + H \quad \text{(R27)}$$

$$H_2O + O(^1D) \rightarrow 2\,OH \quad \text{(R30)}$$

while the most important of them, Reaction (R30), plays only a modest role between 30 and 45 km.

(iv) HO_x that receives the oxygen isotope signature from NO_x:

$$QH + NO \rightleftharpoons OH + NQ \quad \text{(R32)}$$

$$QH + NO_2 \rightleftharpoons OH + NOQ \quad \text{(R33)}$$

while the oxygen isotope composition of NO_x is controlled by reactions with the O_2 and O_3 reservoirs (Sect. 4.4).

6.4.2 The origin of oxygen atoms incorporated in H_2O

On the basis of Sect. 6.4.1, the influence of each oxygen source (O_2, O_3, $O(^1D)$, and NO_x) for the oxygen isotope composition of freshly produced H_2O is assessed. As demonstrated in Fig. 8 and listed in Table 6, molecular oxygen clearly dominates as source of oxygen atoms transferred to water vapour in the entire middle atmosphere. In the model base run (R38 to R41 are omitted), of all oxygen isotopes incorporated in H_2O in stratosphere and mesosphere, respectively, ∼78% and ∼70% stem from O_2, ∼17% and ∼30% from O_3, ∼2% and ∼0% from $O(^1D)$, and ∼2% and ∼0% from other gases such as HNO_3 or H_2O itself (Fig. 8). Another interesting feature is that in the stratosphere ∼50% of the overall oxygen isotope transfer to H_2O proceeds in two steps, that is from O_2 and O_3 to NO_x and then from NO_x via HO_x to H_2O.

This oxygen isotope source partitioning (Fig. 8, Table 6) is reflected in the strongly structured vertical profiles of $\delta^{17}O(H_2O)$ and $\delta^{18}O(H_2O)$ of freshly produced H_2O (Fig. 9). Two maxima occur, both due to oxygen atom transfer from O_3 to H_2O. In the stratosphere, it is the oxygen transfer chain $O_3 \xrightarrow{O} NO_x \xrightarrow{O} HO_x \xrightarrow{O} H_2O$. In the mesosphere with the high concentrations of atomic hydrogen, it is caused by $H+O_3 \rightarrow OH+O_2$ (Reaction R14) and subsequent O transfer from OH to H_2O.

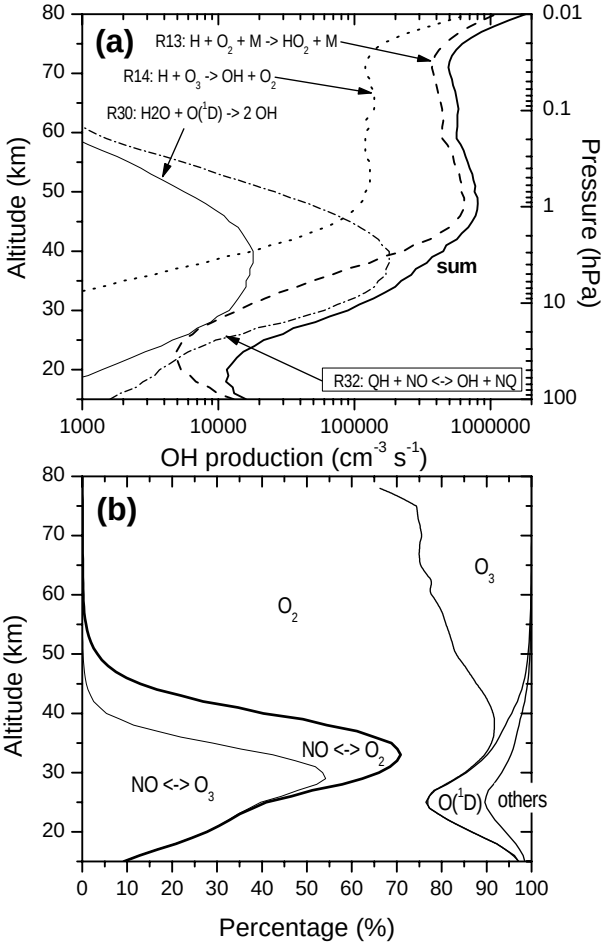

Fig. 8. **(a)** Four most important reactions that lead to the formation of new OH bonds. **(b)** Percentage fraction of oxygen atoms originating from the "reservoirs" O_2, O_3, and $O(^1D)$ in freshly produced H_2O. Thick straight lines separate the three different reservoirs. In the stratosphere, considerable oxygen transfer from O_2 and O_3 to H_2O occurs via the NO_x family (grey areas).

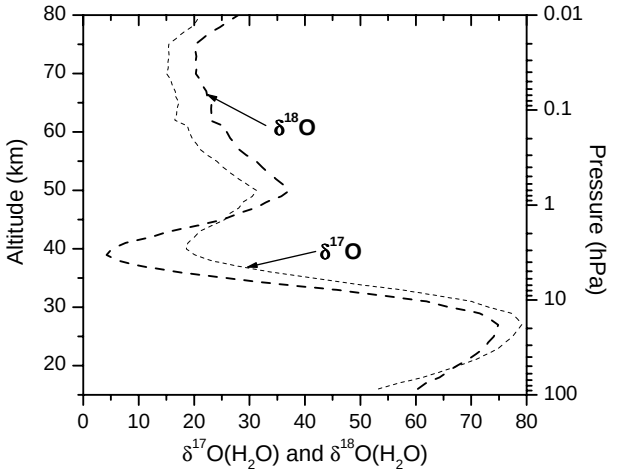

Fig. 9. Vertical profiles of $\delta^{17}O(H_2O)$ and $\delta^{18}O(H_2O)$ of freshly produced H_2O.

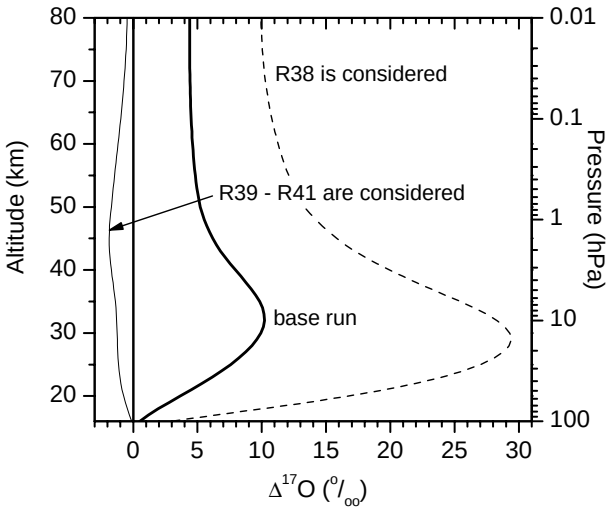

Fig. 10. Calculated vertical profile of $\Delta^{17}O(H_2O)$. Thick straight line: base run. Dashed line: Oxygen exchange reaction (R38) ($NOQ+H_2O \rightleftharpoons NO_2+H_2Q$) is considered at its estimated upper limit. Thin straight line: Oxygen exchange reactions (R39) ($QH+O_2 \rightleftharpoons OH+OQ$) and (R40) ($HOQ+O_2 \rightleftharpoons HO_2+OQ$) are considered at their estimated upper limits.

6.4.3 $\Delta^{17}O(H_2O)$ as a tracer of MIF transfer from O_3 to H_2O

The last Sect. 6.4.2 revealed that the pathway of MIF from O_3 to H_2O is different compared to the one from O_3 to CO_2. CO_2 is assumed to receive the MIF signal exclusively from $O(^1D)$ (produced by the photolysis of O_3) via the short-lived intermediate CO_3' (Yung et al., 1991, 1997; Barth and Zahn, 1997). In the case of H_2O, $O(^1D)$ is only weakly involved in the oxygen isotope transfer (Table 6). In the stratosphere water vapour receives only ∼15% of its MIF signal from $O(^1D)$. In the mesosphere $O(^1D)$ does not play any role at all.

As indicated in Fig. 8, in the stratosphere MIF transfer from O_3 to H_2O basically proceeds in three steps, first MIF transfer from O_3 to NO_x species (via reaction NO-1: $NO+O_3 \longrightarrow NO_2+O_2$, Sect. 4.5), then from NO_x to OH_x and finally transfer to H_2O due to H-abstraction by OH. This quite efficient oxygen transfer chain leads to peaking $\Delta^{17}O(H_2O)$ values of ∼10‰ around ∼32 km altitude (Fig. 10). In the mesosphere, NO_x species are not involved. There, the entire MIF transfer from O_3 to HO_x (and from there to H_2O) proceeds via Reaction (R14): $H+O_3 \longrightarrow OH+O_2$.

6.5 Sensitivity study: Influence of additional oxygen isotope exchange reactions

The results discussed so far constitutes the "base run" in which the already quantified (oxygen) isotope exchange reactions (R32) to (R37) (Table 5) were considered. The last Sect. 6.4 actually revealed the importance of the oxygen isotope exchange reaction (R32) (see Fig. 8) for the oxygen isotope composition of OH and thus freshly produced H_2O.

If the three further, still unquantified exchange reactions with the O_2 reservoir (R39) to (R41) are considered at their estimated upper limit (Table 5), $\delta^{17}O$ and $\delta^{18}O$ of water vapour (and OH) are slightly lower (thin lines in Fig. 4), but the MIF signal is completely washed out (Fig. 10).

On the contrary, if the isotope exchange reaction (R38) ($NOQ+H_2O \rightleftharpoons NO_2+H_2Q$) is considered at the rate measured forty years ago by Jaffe and Klein (1966), the enrichment in $\delta^{17}O$ and $\delta^{18}O$ (Fig. 4) as well as the MIF signal (Fig. 10) strongly increases in the stratosphere and reaches values of $\Delta^{17}O(H_2O) \approx 30‰$ at ∼29 km altitude.

This strong sensitivity to isotope exchange reactions documents the urgent need for better quantified rate constants of the relevant reactions.

7 Conclusions

Application of a simple 1-D isotope chemistry box model demonstrates that a significant number of chemical reactions with diverse gases cause considerable fractionation of all three stable isotope ratios D/H, $^{17}O/^{16}O$, and $^{18}O/^{16}O$ in middle atmospheric water vapour relative to values at the tropopause. This makes a description much more complicated compared to other trace gases such as CO_2, CH_4, and N_2O.

$\delta D(H_2O)$ was modelled to increase from –660‰ at the tropopause to –410‰ above 40 km, which is in excellent agreement with the observations. This increase by ∼250‰ corresponds to a fraction of ∼40% of H_2O produced as end product of the oxidation of CH_4. Although the D fractionation factors of the individual CH_4 oxidation reactions with OH, $O(^1D)$, and Cl differ strongly, the $\delta D(H_2O)$ value turned out to be no sensitive tracer to distinguish between

the different CH_4 oxidation chains. This has two reasons. First, the major CH_4 loss occurs in the middle and upper stratosphere where the reactions with $O(^1D)$ which comes along with weak isotope fractionation dominates. Second, the chemical lifetime of H_2O is long in the middle atmosphere. This allows for significant redistribution and thus weakening of spatial gradients of $\delta D(H_2O)$.

The results for the oxygen isotope ratios $^{17}O/^{16}O$, and $^{18}O/^{16}O$ are less robust, because of the many reactions involved in the oxygen isotope transfer from the reservoirs to H_2O and the many badly or not quantified isotope fractionation factors and oxygen isotope exchange reactions. In the base run, where the Reactions (R38), (R39) and (R40) are not considered, $\delta^{17}O(H_2O)$ and $\delta^{18}O(H_2O)$ are calculated to increase relative to the tropopause by up to ∼85‰ and ∼145‰, respectively, which is also in agreement with the observations. Fractionation of the oxygen isotope ratios in H_2O was demonstrated to be determined almost exclusively by the isotope signature of OH. The oxygen isotopic composition of OH, in turn, is mainly controlled by the one of O_2 that is mass-dependently fractionated (MDF). In the stratosphere and mesosphere, respectively, ∼78 and ∼70% of all oxygen atoms transferred to H_2O stem from O_2, while ∼17 and ∼30% originate from O_3 that is mass-independently fractionated (MIF). As a result, the calculated MIF signal of H_2O is only modest and reaches values of $\Delta^{17}O(H_2O)$=10‰ at 30–35 km altitude.

However, if beyond the base run, further badly quantified oxygen isotope exchange reactions with O_2 (R39 and R40) are considered at their estimated upper limit, the MIF signature completely vanishes in middle atmospheric H_2O. In contrast, if the isotope exchange reaction of H_2O with NO_2 (Reaction R38) is considered, the MIF signal reaches high values of $\Delta^{17}O(H_2O)$=30‰ around 29 km. Indeed and in any case, the transfer of the MIF signature in O_3 to OH and H_2O proceeds primarily via NO_x species in the stratosphere and directly via the reaction of $H+O_3 \rightarrow OH+O_2$ in the mesosphere. That is, the MIF transfer from O_3 to H_2O is quite different from the one from O_3 to CO_2 where it proceeds via $O(^1D)$ and the intermediate complex CO_3^*.

The largest unknowns in our calculations are the unquantified reaction rates of a few oxygen isotope exchange reactions, in particular of OH_x and NO_x with O_2, and the many unquantified isotope fractionation factors of the reactions involved in the isotope transfer to H_2O. In this respect, the most urgent need in this research field is the development of more precise techniques to measure the isotope composition of water vapour both in the laboratory and atmosphere.

Finally, the calculated MIF signal transferred to HO_x and thus to H_2O is only half as large as the one determined by Lyons (2001). This discrepancy arises from the different $\Delta^{17}O$ signatures assumed for the asymmetric O_3 molecule and $O(^1D)$. Lyons (2001) used (i) the branching ratios of 0.43 and 0.57 for $\delta^{18}O$ in the reaction of $O+QO \longrightarrow OQO$ and QOO as measured by Janssen et al. (1999) for $\delta^{17}O$, too, and (ii) the isotope fractionation factors for this reaction measured by Mauersberger et al. (1999). This assumption led to $\Delta^{17}O$ values of asymmetric O_3 of $\Delta^{17}O(QOO)$=∼85‰, and together with the mean $\Delta^{17}O$ values of O_3 of $\Delta^{17}O(O_3)$=∼38‰, to $\Delta^{17}O$ values of symmetric O_3 of $\Delta^{17}O(OQO))$=−50‰ only (because $\Delta^{17}O(O_3)$=2/3 $\Delta^{17}O(QOO)$+1/3 $\Delta^{17}O(OQO)$). Such a strong difference in $\Delta^{17}O$ between asymmetric and symmetric ozone is unlikely (C. Janssen, personal communication). In contrast, we assumed identical ratios of the enrichments of $\delta^{17}O$ and $\delta^{18}O$ in QOO and OQO. That is, in the stratosphere we apply mean $\Delta^{17}O$ values of 34‰ for O_3, which is in agreement with Lyons (2001), but $\Delta^{17}O$ values of 39‰ for QOO and 25‰ for OQO.

Acknowledgements. We thank U. Platt for his scientific assistance during the early preparation phase.

Edited by: U. Pöschl

References

Anderson, S. M., Morton, J., and Mauersberger, K.: Laboratory measurements of ozone isotopomeres by tunable diode laser absorption spectroscopy, Chem. Phys. Lett., 156, 175–180, 1989.

Baertschi, P.: Absolute ^{18}O content of standard mean ocean water, Earth and Plan. Sci. Lett., 31, 341–344, 1976.

Barth, V. and Zahn, A.: Oxygen isotope composition of carbon dioxide in the middle atmosphere, J. Geophys. Res., 102, 12 995–10 007, 1997.

Brasseur, G. P. and Solomon, S.: Aeronomy of the middle atmosphere, D. Reidel Publishing Company, Dordrecht/Boston/Lancaster/Tokyo, 1986.

Cliff, S. S. and Thiemens, M. H.: The $^{18}O/^{16}O$ and $^{17}O/^{16}O$ ratios in atmospheric nitrous oxide: A mass-independent anomaly, Science, 278, 1774–1775, 1997.

Cliff, S. S., Brenninkmeijer, C. A. M., and Thiemens, M. H.: First measurement of the $^{18}O/^{16}O$ and $^{17}O/^{16}O$ ratios in stratospheric nitrous oxide: A mass-independent anomaly, J. Geophys. Res., 104, 16 171–16 175, 1999.

Coplen, T. B., Bohlke, J. K., De Bievre, P., Ding, T., Holden, N. E., Hopple, J. A., Krouse, H. R., Lamberty, A., Peiser, H. S., Revesz, K., Rieder, S. E., Rosman, K. J. R., Roth, E., Taylor, P. D. P., Vocke, R. D., and Xiao, Y. K.: Isotope-abundance variations of selected elements (IUPAC Technical Report), Pure Appl. Chem., 74, 10, 1987–2017, 2002.

Craig, H.: Standard for reporting concentrations of deuterium and oxygen-18 in natural waters, Science, 133, 1833–1834, 1961.

Crutzen, P. J.: Methane's sinks and sources, Nature, 350, 380–381, 1991.

Crutzen, P. J.: On the role of CH_4 in atmospheric chemistry: sources, sinks and possible reductions in anthropogenic sources, Ambio, 24, 52–55, 1995.

DeMore, W. B., Howard, C. J., Sander, S. P., Ravishankara, A. R., Golden, D. M., Kolb, C. E., Hampson, R. F., Molina, M. J., and Kurylo, M. J.: Chemical kinetics and photochemical data for use in stratospheric modeling, Pasadena, CA: JPL Publication 97-4, 1997.

Dessler, A. E., Weinstock, E. M., Anderson, J. G., and Chan, K. R.: Mechanisms controlling water vapor in the lower stratosphere: A tale of two stratospheres, J. Geophys. Res., 100, 23 167–23 172, 1995.

Dessler, A. E. and Sherwood, S. C.: A model of HDO in the tropical tropopause layer, Atmos. Chem. Phys., 3, 2173–2181, 2003, mboxhttp://www.atmos-chem-phys.net/3/2173/2003/.

DeWit J. C., Van der Straaten, C. M., and Mook, W. G.: Determination of the absolute D/H ratio of V-SMOW and SLAP, Geostand. Newslett., 4, 33–36, 1980.

Dinelli, B. M., Lepri, G., Carlotti, M., Carli, B., Mencaraglia, F., Ridolfi, M., Nolt, I. G., and Ade, P. A. R.: Measurements of the isotope ratio distribution of $HD^{16}O$ and $H_2^{18}O$ in the 20–38 km altitude range from far-infrared spectra, Geophys. Res. Lett., 24, 2003–2006, 1997.

Dinelli, B. M., Carli, B., and Carlotti, M.: Measurement of stratospheric distribution of $H_2^{16}O$, $H_2^{18}O$, $H_2^{17}O$ and $HD^{16}O$ from far infrared spectra, J. Geophys. Res., 96, 7509–7514, 1991.

Dubey, K., Mohrschladt, R., Donahue, N. M., and Anderson, J. G.: Isotope specific kinetics of hydroxyl radical (OH) with water (H_2O): Testing models of reactivity and atmospheric fractionation, J. Phys. Chem., 101, 1494–1500, 1997.

Engel, A., Schiller, C., Schmidt, U., Borchers, R., Ovarlez, H., and Ovarlez, J.: The total hydrogen budget in the Arctic winter stratosphere during EASOE, J. Geophys. Res., 101, 14 495–14 503, 1996.

Feilberg, K. L., Johnson, M. S., and Nielsen, C. J.: Relative reaction rates of HCHO, HCDO, DCDO, $H^{13}CHO$, and $HCH^{18}O$ with OH, Cl, Br, and NO_3 radicals, J. Phys. Chem., 108, 7393-7398, 2004.

Forster, P. M. de F. and Shine, K. P.: Stratospheric water vapour changes as a possible contributor to observed stratospheric cooling, Geophys. Res. Lett., 26, 3309–3312, 1999.

Forster, P. M. de F. and Shine, K. P.: Assessing the climate impacts of trends in stratospheric water vapor, Geophys. Res. Lett., 29, doi:10.1029/2001GL013909, 2002.

Franz, P. and Röckmann, T.: High-precision isotope measurements of $H_2^{16}O$, $H_2^{17}O$, $H_2^{18}O$, and the ^{17}O-anomaly of water vapor in the southern lowermost stratosphere, Atmos. Chem. Phys., 5, 2949–2959, 2005, mboxhttp://www.atmos-chem-phys.net/5/2949/2005/.

Friedmann, I. and Scholz, T. G.: Isotopic composition of atmospheric hydrogen, 1967–1969, J. Geophys. Res., 79, 785–788, 1974.

Froidevaux, L. and Yung, Y. L.: Radiation and chemistry in the stratosphere: Sensitivity to O_2-absorption cross sections in the Herzberg continuum, Geophys. Res. Lett., 9, 854–857, 1982.

Gettelman, A., Holton, J. R., and Rosenlof, K. H.: Mass fluxes of O_3, CH_4, N_2O and CF_2Cl_2 in the lower stratosphere calculated from observational data, J. Geophys. Res., 102, 19 149–19 159, 1997.

Gierczak, T., Talukdar, R. K., Herdon, S., Vaghjiani, G. L., and Ravishankara, A. R.: Rate coefficients for the reactions of hydroxyl radicals with methane and deuterated methanes, J. Phys. Chem., 101, 3125–3134, 1997.

Greenblatt, G. D. and Howard, C. J.: Oxygen Atom Exchange in the Interaction of ^{18}O with Several Small Molecules, J. Phys. Chem., 93, 1035–1042, 1989.

Groo, J.-U.: Modelling of stratospheric chemistry based on HALOE/UARS satellite data, PhD thesis, University of Mainz, Verlag Shaker, Aachen, 1996.

Günther, J., Erbacher, B., Krankowsky, D., and Mauersberger, K.: Pressure dependence of two relative ozone formation rate coefficients, Chem. Phys. Lett., 306, 209–213, 1999.

Guo, J., Abbas, M. M., and Nolt, I. G.: Stratospheric $H_2{}^{18}O$ distribution from infrared observations, Geophys. Res. Lett., 16, 1277–1280, 1989.

Hagemann, R., Nier, G., and Roth, E.: Absolute isotopic scale for deuterium analysis of natural waters. Absolute D/H ratio for SMOW, Tellus, 22, 712–715, 1970.

Holdsworth, G., Fogarasi, S., and Krouse, H. R.: Variation of stable isotopes of water with altitude in the Saint Elias Mountains of Canada, J. Geophys. Res., 96, 7483–7494, 1991.

Holton, J. R., Haynes, P. H., McIntyre, M. E., Douglass, A. R., Rodd, R. B., and Pfister, L.: Stratosphere-troposphere exchange, Rev. Geophys., 33, 403–439, 1995.

Hurst, D. F., Dutton, G. S., Romashkin, P. A., Wamsley, P. R., Moore, F. L., Elkins, J. W., Hintsa, E. J., Weinstock, E. M., Herman, R. L., Moyer, E. J., Scott, D. C., May, R. D., and Webster, C. R.: Closure of the total hydrogen budget of the northern extratropical lower stratosphere, J. Geophys. Res., 104, 8191–8200, 1999.

IPCC, Climate Change 2001: The Scientific Basis, Contribution of Working Group I to the Third Assessment Report of the Intergovernmental Panel on Climate Change (IPCC), edited by: Houghton, J. T., Ding, Y., Griggs, D. J., Noguer, M., van der Linden, P. J., and Xiaosu, D., Cambridge University Press, UK, pp. 944, 2001.

Janssen, C., Guenther, J., Krankowsky, D., and Mauersberger, K.: Relative formation rates of $^{50}O_3$, and $^{52}O_3$ in ^{16}O–^{18}O mixtures, J. Chim. Phys., 111, 7179–7182, 1999.

Johnson, D. G., Jucks, K. W., Traub, W. A., and Chance, K. V.: Isotopic composition of stratospheric ozone, J. Geophys. Res., 105, 9025–9031, 2000.

Johnson, D. G., Jucks, K. W., Traub, W. A., and Chance, K. V.: Isotopic composition of stratospheric water vapor: Measurements and photochemistry, J. Geophys. Res., 106, 12 211–12 218, 2001a.

Johnson, D. G., Jucks, K. W., Traub, W. A., and Chance, K. V.: Isotopic composition of stratospheric water vapor: Implications for transport J. Geophys. Res., 106, 12 219–12 226, 2001b.

JPL (Ed.): Chemical Kinetics and Photochemical Data for Use in Atmospheric Studies, JPL, 2003.

Kaiser, J. and Röckmann, T.: Absence of isotope exchange in the reaction of N_2O+$O(^1D)$ and the global ^{17}O budget of nitrous oxide, Geophys. Res. Lett.,, 32, L15808, doi:10.1029/2005GL023199, 2005.

Kaye, J. A. and Strobel, D. F.: Enhancement of heavy ozone in the Earth's atmosphere?, J. Geophys. Res., 88, 8447–8452, 1983

Kaye, J. A.: Analysis of the origins and implications of the ^{18}O content of stratospheric water vapour, J. Atmos. Chem., 10, 39–51, 1990.

Keith, D. W.: Stratospheric-tropospheric exchange: Inferences from the isotopic composition of water vapour, J. Geophys. Res., 105, 15 167–15 173, 2000.

Khalil, M. A. K., Khalil, M. A. K., Shearer, M. J., and Rasmussen, R. A.: Methane sinks and distribution, in: Atmospheric Methane: Sources, Sinks, and Role in Global Change, edited by: Khalil, M.

A. K., NATO ASI Ser. I, 13, Springer-Verlag, New York, 1993.

Kirk-Davidoff, D. B., Hintsa, E. J., Anderson, J. G., and Keith, D. W.: The effect of climate change on ozone depletion through changes in stratospheric water vapour, Nature, 402, 399–401, 1999.

Kuang, Z., Toon, G. C., Wennberg, P. O., and Yung, Y. L.: Measured HDO/H_2O ratios across the tropical tropopause, Geophys. Res. Lett., 30(7), 1372, doi:10.1029/2003GL017023, 2003.

Lary, D. J. and Toumi, T.: Halogen-catalyzed methane oxidation, J. Geophys. Res., 102, 23 421–23 428, 1997.

Lelieveld, J. and Crutzen, P. J.: Influences of cloud photochemical processes on tropospheric ozone, Nature, 343, 227–233, 1990.

Lelieveld, J. and Crutzen, P. J.: Role of deep convection in the ozone budget of the troposphere, Science, 264, 1759–1761, 1994.

Lelieveld, J., Crutzen, P. J., and Dentener, F. J.: Changing concentration, lifetime and climate forcing of atmospheric methane, Tellus, 50B, 128–150, 1998

Le Texier, H., Solomon, S., and Garcia, R. R.: The role of molecular hydrogen and methane oxidation in the water vapour budget of the stratosphere, Quart. J. Roy. Meteorol. Soc., 114, 281–295, 1988.

Li, W., Baoling, N., Deqiu, J., and Qingliang, Z.: Measurement of the absolute abundance of oxygen-17 in VSMOW, Kexue Tongbao (Chinese Science Bulletin), 33, 1610–1613, 1988.

López-Valverde, M. A., López-Puertas, M., Remedios, J. J., Rodgers, C. D., Taylor, F. W., Zipf, E. C., and Erdman, P. W.: Validation of measurements of carbon monoxide from the improved stratospheric and mesospheric sounder, J. Geophys. Res., 101, 9929–9955, 1996.

Luz, B., Barkan, E., Bender, M. L., Thiemens, M. H., and Boering, K. A.: Triple-isotope composition of atmospheric oxygen as a tracer of biosphere productivity, Nature, 400, 547–550, 1999.

Luz, B. and Barkan, E.: Assessment of oceanic productivity with the triple-isotope composition of dissolved oxygen, Science, 288(5473), 2028–2031, 2000.

Lyons, J. R.: Transfer of mass-independent fractionation in ozone to other oxygen-containing radicals in the atmosphere, Geophys. Res. Lett., 28, 3231–3234, 2001.

Masgrau, L., González-Lafont, A., and Lluch, J. M.: Mechanism of the gas-phase HO+H2$_O$→H_2O+OH reaction and several associated isotope exchange reactions: A canonical variational transition state theory plus multidimensional tunneling calculation, J. Phys. Chem.A, 103, 1044–1053, 1999.

Massie S. T. and Hunten, D. M.: Stratospheric eddy diffusion coefficients from tracer data, J. Geophys. Res., 86, 9859–9868, 1981.

Mauersberger, K., Erbacher, B., Krankowsky, D., Günther, J., and Nickel, R.: Ozone isotope enrichment: Isotopomer-Specific rate coefficients, Science, 283, 370–372, 1999.

Mauersberger, K., Lämmerzahl, P., and Krankowsky, D.: Stratospheric ozone isotope enrichments – revisited, Geophys. Res. Lett., 28, 3155–3158, 2001.

McCarty, M. C., Boering, K. A., Rahn, T., Eiler, J. M., Rice, A. L., Tyler, S. C., Schauffler, S., Atlas, E., and Johnson, D. G.: The hydrogen isotopic composition of water vapor entering the stratosphere inferred from high-precision measurements of δD-CH_4 and δD-H_2, J. Geophys. Res., 109, doi:10.1029/2003JD004003, 2004.

Michelsen, H. A., Irion, F. W., Manney, G. L., Toon, G. C., and Gunson, M. R.: Features and trends in Atmospheric Trace Molecules Spectroscopy (ATMOS) version 3 stratospheric water vapor and methane measurements, J. Geophys. Res., 105, 11 713–22 724, 2000.

Morton, J., Barnes, J., Schueler, B., and Mauersberger, K.: Laboratory studies of heavy ozone, J. Geophys. Res., 95, 901–907, 1990.

Moyer, E. J., Irion, F. W., Yung, Y. L., and Gunson, M. R.: ATMOS stratospheric deuterated water and implications for troposphere-stratosphere transport, Geophys. Res. Lett., 23, 2385–2388, 1996.

Oltmans, S. J. and Hofmann, D. J.: Increase in lower-stratospheric water vapour at a mid-latitude Northern Hemisphere site from 1981 to 1994, Nature, 374, 146–149, 1995.

Pollock, W., Heidt, L. E., Lueb, R., and Ehhalt, D. H.: Measurement of stratospheric water vapour by cryogenic collection, J. Geophys. Res., 85, 5555–5568, 1980.

Quay, P., Stutsman, J., Wilbur, D., Snover, A., Dlugokencky, E., and Brown, T.: The isotopic composition of atmospheric methane, Global Biogeochem. Cycles, 13, 445–461, 1999.

Rahn, T., Eiler, J. M., Boering, K. A., Wennberg, P. O., McCarthy, M. C., Tyler, S., Schauffler, S., Donnelly, S., and Atlas, E.: Extreme deuterium enrichment in stratospheric hydrogen and the global atmospheric budget of H_2, Nature, 424, 918–921, 2003.

Randel, W. J., Wu, F., Gettelmann, A., Russell III, J. M., Zawodny, J. M., and Oltmans, S. J.: Seasonal variation of water vapor in the lower stratosphere observed in Halogen Occultation Experiment data, J. Geophys. Res., 106, 14 313–14 325, 2001.

Rhee, T. S., Brenninkmeijer, C. A. M., and Röckmann, T.: The overwhelming role of soils in the global atmospheric hydrogen cycle, Atmos. Chem. Phys., 6, 1611–1625, 2006, mboxhttp://www.atmos-chem-phys.net/6/1611/2006/.

Ridal, M., Jonsson, A., Werner, M., and Murtagh, D. P.: A one-dimensional simulation of the water vapor isotope HDO in the tropical stratosphere, J. Geophys. Res., 106, 32 283–32 294, 2001.

Ridal, M.: Isotopic ratios of water vapor and methane in the stratosphere: comparison between ATMOS measurements and a one-dimensional model, J. Geophys. Res., 107, doi:10.1029/2001JD000708, 2002.

Rinsland, C. P., Gunson, M. R., Foster, J. C., Toth, R. A., Farmer, C. B., and Zander, R.: Stratospheric profiles of heavy water vapour isotopes and CH_3D from analysis of the ATMOS Spacelab 3 infrared solar spectra, J. Geophys. Res., 96, 1057–1068, 1991.

Rinsland, C. P., Goldman, A., Malathy Devi, V., Fridovich, B., Snyder, D. G. S., Jones, G .D., Murcray, F .J., Murcray, D. G., Smith, M. A. H., Seals Jr., R. K., Coffey, M. T., and Mankin, W. G.: Simultaneous stratospheric measurements of H_2O, HDO, CH_4 from balloon-borne and aircraft infrared solar absorption spectra and tunable diode laser spectroscopy of HDO, J. Geophys. Res., 89, 7259–7266, 1984.

Röckmann, T., Kaiser, J., Brenninkmeijer, C. A. M., Crowley, J. N., Borchers, R., Brand, W. A., and Crutzen, P. J.: Isotopic enrichment of nitrous oxide ($^{15}N^{14}NO$, $^{14}N^{15}NO$, $^{14}N^{14}N^{18}O$) in the stratosphere and in the laboratory, J. Geophys. Res., 106, 10 403–10 410, 2001.

Röckmann, T., Kaiser, J., Crowley, J. N., Brenninkmeijer, C. A. M., and Crutzen, P. J.: The origin of the anomalous or "mass-independent" oxygen isotope fractionation in atmospheric N_2O, Geophys. Res. Lett., 28, 503–506, 2001.

Rozanski, K., Araguas-Araguas, L., and Gonfiantini, R.: Isotopic patterns in modern global precipitation, Climate change in continental isotopic records, Geophys. Monograph, 78, 1–36, 1993.

Rosenlof, K. H., Tuck, A. F., Kelly, K. K., Russell III, J. M., and McCormick, M. P.: Hemispheric asymmetries in water vapour and inferences about transport in the lower stratosphere, J. Geophys. Res., 102, 13 213–13 234, 1997.

Rosenlof, K. H., Oltmans, S. J., Kley, D., Russell, J. M., Chiou, E. W., Chu, W. P., Johnson, D. G., Kelly, K. K., Michelsen, H. A., Nedoluha, G. E., Remsberg, E. E., Toon, G. C., and McCormick, M. P.: Stratospheric water vapor increases over the past half-century, Geophys. Res. Lett., 1195–1198, 2001.

Rosenlof, K. H.: Transport changes inferred from HALOE water and methane measurements, J. Meteorol. Soc. Jpn., 80, 4B, 831–848, 2002.

Saueressig, G., Bergamaschi, P., Crowley, J. N., and Fischer, H.: D/H kinetic isotope effect in the reaction CH_4+Cl, Geophys. Res. Lett., 23, 3619–3622, 1996.

Saueressig, G., Crowley, J. N., Bergamaschi P., Brühl, C., Brenninkmeijer, C. A. M., and Fischer, H.: Carbon 13 and D kinetic isotope effects in the reactions of CH_4 with $O(^1D)$ and OH: New laboratory measurements and their implications for the isotopic composition of stratospheric methane, J. Geophys. Res., 106, 23 127–23 138, 2001.

Sharma, H. D., Jervis, R. E., and Wong, K. Y.: Isotopic exchange reactions in nitrogen oxides, J. Phys. Chem., 74, 923–933, 1970.

Smith, R. B.: Deuterium in North Atlantic storm tops, J. Atmos. Sci., 49, 2041–2057, 1992.

SPARC: SPARC assessment of upper tropospheric and stratospheric water vapour, edited by: Kley, D., Russell III, J. M., and Phillips, C., SPARC report No. 2, 2000.

Stowasser, M., Oelhaf, H., Wetzel, G., Friedl-Vallon, F., Maucher, G., Seefeldner, M., Trieschmann, O., and Clarmann, T. V.: Simultaneous measurements of HDO, H_2O, and CH_4 with MIPAS-B: Hydrogen budget and indication of dehydration inside the polar vortex, J. Geophys. Res., 104, 19 213–19 225, 1999.

Talukdar, R. K. and Ravishankara, A. R.: Rate coefficients for $O(^1D)$+H_2, D_2, HD reactions and H atom yield in $O(^1D)$+HD reaction, Chem. Phys. Lett., 253, 177–183, 1996.

Taylor, C. B.: Vertical distribution of deuterium in atmospheric water vapour: problems in application to assess atmospheric condensation models, Tellus, 36B, 67–72, 1984.

Thiemens, M. H. and Heidenreich III, J. E.: The mass-independent fractionation of oxygen: A novel isotope effect and its possible cosmochemical implications, Science, 219, 1073–1075, 1983.

Thiemens, M. H. and Jackson, T.: New experimental evidence for the mechanism for production of isotopically heavy ozone, Geophys. Res. Lett., 15, 639–642, 1988.

Thiemens, M. H. and Jackson, T.: Pressure dependency for heavy isotope enhancement in ozone formation, Geophys. Res. Lett., 17, 717–719, 1990.

Tse, R. S., Wong, S. C., and Yuen, C. P.: Determination of deuterium/hydrogen ratios in natural waters by Fourier transform nuclear magnetic resonance spectrometry, Anal. Chem., 52, 2445–2447, 1980.

Tyler, S. C., Ajie, H. O., Rice, A. L., Cicerone, R. J., and Tuazon, E. C.: Experimentally determined kinetic isotope effects in the reaction of CH_4 with Cl: Implications for atmospheric CH_4, Geophys. Res. Lett., 27, 1715–1718, 2000.

Webster, C. R. and Heymsfield, A. J.: Water Isotope Ratios D/H, $^{18}O/^{16}O$, $^{17}O/^{16}$ in and out of Clouds Map Dehydration Pathways, Science, 302, 1742–1745, 2003.

Wen, J. and Thiemens, M. H.: Multi-isotope study of the $O(^1D)$+CO_2 exchange and stratospheric consequences, J. Geophys. Res., 98, 12 801–12 808, 1993.

Yang, H. and Tung, K. K.: Cross-isentropic stratosphere-troposphere exchange of mass and water vapour, J. Geophys. Res., 101, 9413–9423, 1996.

Yung, Y. L., DeMore, W. B., and Pinto, J. P.: Isotope exchange between carbon dioxide and ozone via $O(^1D)$ in the stratosphere, Geophys. Res. Lett., 18, 13–16, 1991.

Yung, Y. L., Lee, A. Y. T., Irion, F. W., DeMore, W. B., and Wen, J.: Carbon dioxide in the atmosphere: Isotopic exchange with ozone and its use as tracer in the middle atmosphere, J. Geophys. Res., 102, 10 857–10 866, 1997.

Zahn, A.: Constraints on 2-way transport across the Arctic tropopause based on O_3, stratospheric tracer (SF_6) ages, and water vapor isotope (D, T) tracers, J. Atmos. Chem., 39, 303–325, 2001.

Zahn, A., Barth, V., Pfeilsticker, K., and Platt, U.: Deuterium, Oxygen-18 and tritium as tracers for water vapour transport in the lower stratosphere and tropopause region, J. Atmos. Chem., 30, 25–47, 1998.

Zöger, M., Engel, A., McKenna, D. S., Schiller, C., Schmidt, U., and Woyke, T.: Balloon-borne in situ measurements of stratospheric H_2O, CH_4 and H_2 in midlatitudes, J. Geophys. Res., 104, 1817–1825, 1999.